Climate
of the Past

Contrasts in the marine inorganic carbon chemistry of the Benguela Upwelling System since the Last Glacial Maximum

Szabina Karancz[1], Lennart J. de Nooijer[1], Bas van der Wagt[1], Marcel T. J. van der Meer[2], Sambuddha Misra[3], Rick Hennekam[1], Zeynep Erdem[2], Julie Lattaud[4], Negar Haghipour[5,6], Stefan Schouten[2,7], and Gert-Jan Reichart[1,7]

[1]Department of Ocean Systems, NIOZ Royal Netherlands Institute for Sea Research, Texel, the Netherlands
[2]Department of Marine Microbiology and Biogeochemistry, NIOZ Royal Netherlands Institute for Sea Research, Texel, the Netherlands
[3]Centre for Earth Sciences, Indian Institute of Science, Bengaluru, India
[4]Department of Environmental Sciences, University of Basel, Basel, Switzerland
[5]Geological Institute, Department of Earth Sciences, ETH Zürich, Zürich, Switzerland
[6]Laboratory of Ion Beam Physics, ETH Zürich, Zürich, Switzerland
[7]Department of Earth Sciences, Faculty of Geosciences, Utrecht University, Utrecht, the Netherlands

Correspondence: Szabina Karancz (szabina.karancz@nioz.nl)

Abstract. Upwelling regions are dynamic systems where relatively cold, nutrient-, and CO_2-rich waters reach to the surface from the deep. CO_2 sink or source properties of these regions are dependent not only on the dissolved inorganic carbon content of the upwelled waters, but also on the efficiency of the biological carbon pump which constrains the drawdown of atmospheric CO_2 in the surface waters. The Benguela Upwelling System (BUS) is a major upwelling region with one of the most productive marine ecosystems today. However, contrasting signals reported on the variation in upwelling intensities based on, for instance, foraminiferal and radiolarian indices over the last glacial cycle indicate that a complete understanding of (local) changes is currently lacking. To reconstruct changes in the CO_2 history of the northern Benguela upwelling region over the last 27 kyr, we used a box core (64PE450-BC6) and piston core (64PE450-PC8) from the Walvis Ridge. Here, we apply various temperature and pCO_2 proxies, representing both surface ($U_{37}^{K'}$ and $\delta^{13}C$ of alkenones) and subsurface (Mg / Ca and $\delta^{11}B$ in planktonic foraminiferal shells) processes. Reconstructed pCO_2 records suggest enhanced storage of carbon at depth during the Last Glacial Maximum (LGM). The offset between $\delta^{13}C$ of planktonic (high $\delta^{13}C$) and benthic foraminifera (low $\delta^{13}C$) suggests evidence of a more efficient biological carbon pump, potentially fueled by remote

and local iron supply through eolian transport and dissolution in the shelf regions, effectively preventing release of the stored glacial CO_2.

1 Introduction

Upwelling systems are crucial components in the global carbon cycle thanks to intense biogeochemical cycling and enhanced biological productivity (Turi et al., 2014). Upwelling zones return the cold, nutrient-, and CO_2-rich waters from depth to the surface, which is also reflected in regional changes in surface water inorganic carbon chemistry. The connection between the deep and surface ocean thereby provides a potential mechanism linking changes in ocean circulation and chemistry with the atmosphere. Still, the shoaling of the thermocline and nutricline in these regions also favors phytoplankton growth to such a degree that these areas represent the majority of the most productive regions of the ocean (Fig. 1a). Thus, the leakage of CO_2 from the depths to the atmosphere is negated by biological sequestration, simultaneously rendering its quantification a challenging undertaking. The surface waters of the upwelling system undergo an increase in the partial pressure of CO_2 (pCO_2) and a decrease in pH due to upwelling of deep CO_2-rich water. In

turn, the enhanced primary productivity due to increased nutrients results in the drawdown of $p\mathrm{CO_2}$ by converting $\mathrm{CO_2}$ into organic carbon, after which it may be returned to the deep ocean via the biological carbon pump (BCP; Volk and Hoffert, 1985; Longhurst and Glen Harrison, 1989; Ducklow et al., 2001; Turi et al., 2014; Hales et al., 2005; Muller-Karger et al., 2005). Ultimately, the net $\mathrm{CO_2}$ flux from the ocean to the atmosphere is a function of the balance between upwelling strength (increase in $\mathrm{CO_2}$) and efficiency of the BCP (drawdown of $\mathrm{CO_2}$). On geological timescales, this efficiency may have varied, potentially modulating local air–sea $\mathrm{CO_2}$ balance (Kohfeld et al., 2005; Kwon et al., 2009; Parekh et al., 2006; Hain et al., 2014).

The efficiency of the BCP determines how much of the newly produced particulate organic carbon at the surface is transported to the deep (Volk and Hoffert, 1985; Hain et al., 2014). During primary production, nutrients are consumed (e.g., nitrate, phosphate; Redfield, 1958) from the surface ocean and dissolved inorganic carbon (DIC) is taken up in organic matter, which is also reflected by the enrichment in $^{13}\mathrm{C}$ of the surface DIC (Degens et al., 1968). This implies that we can use seawater carbon isotopes as a proxy for the efficiency of the BCP. Seawater carbon isotopes can be reconstructed using the carbon isotopic composition ($\delta^{13}\mathrm{C}$) in shells of carbonate producers, such as foraminifera. During high-productivity periods, the enhanced carbon uptake at the sea surface will enrich the shells of planktonic foraminifera in $^{13}\mathrm{C}$. At the same time, the $^{13}\mathrm{C}$-depleted carbon transported to the deep as organic matter will decrease the $^{13}\mathrm{C}$ content of the deep-water DIC pool, resulting in low $\delta^{13}\mathrm{C}$ values in the benthic foraminifera shells (Fig. 1b). Therefore, the stable carbon isotopic composition of these inorganic archives is imprinted by complex processes related to both surface to deep gradients and ocean circulations. Water masses of different origins carry distinct $\delta^{13}\mathrm{C}$ compositions resulting in integrated signatures of air–sea exchange and production/remineralization related to different water masses within the foraminiferal shells. The difference between planktonic and benthic $\delta^{13}\mathrm{C}$, however, also records a measure for the efficiency of the BCP, where more divergent values between the surface and the deep indicate a more efficient BCP (Hilting et al., 2008).

This study focuses on the Benguela Upwelling System (BUS), as it is one of the major upwelling regions, where the strength of the upwelling and productivity changed over glacial–interglacial timescales. Whether upwelling intensity was stronger during glacial periods (Oberhänsli, 1991; Little et al., 1997; Kirst et al., 1999; Mollenhauer et al., 2003) or interglacial periods (Diester-Haass et al., 1992; Des Combes and Abelmann, 2007) is, however, still debated. Inconsistencies in the published body of work are possibly caused by seasonal differences between proxy signal carriers and/or major spatial- (depth-) related gradients, which is especially true for regions with strong $\mathrm{CO_2}$ flux dynamics (Fig. 1c). Exchange of $\mathrm{CO_2}$ between seawater and the atmosphere at these regions may be constrained only by applying multiple proxies that comprise various living depths and seasonal preferences. Therefore, here, we compare organic and inorganic proxies for temperature ($\mathrm{U}^{K'}_{37}$, Mg / Ca) and the carbon system (alkenone $\delta^{13}\mathrm{C}$, foraminiferal $\delta^{11}\mathrm{B}$) with reconstructed efficiency of the BCP in the Benguela upwelling area to unravel the potential role of such areas in known changes in atmospheric $p\mathrm{CO_2}$ on glacial–interglacial timescales. At the same time, this allows us to compare proxies and investigate (in)consistencies between different carbon system and temperature proxies.

2 Oceanographic setting

The BUS is one of the four major eastern boundary upwelling systems, and it is located between 15 and 34° S along the coastline of Africa (Hill, 1998; Hart and Currie, 1960). This region bears the highest productivity today among the eastern boundary upwelling systems, fueled by nutrients transported mainly from the higher latitudes. Advection of the cold and nutrient-rich water is a persistent phenomenon throughout the year (Carr, 2001; Chavez and Messié, 2009), and the magnitude of the particulate organic carbon (POC) flux from the surface to the deep exceeds $20\,\mathrm{gC\,m^{-2}\,yr^{-1}}$ (Henson et al., 2011; Laws et al., 2000; DeVries and Weber, 2017).

The BUS is associated with the South Atlantic anticyclonic gyre, which gives rise to upwelling on its southeastern flank where it meets the African continent (Peterson and Stramma, 1991). The low-pressure system over western South Africa causes a pressure gradient between the continent and the ocean and thereby strengthens the southerly wind stress off the coast of Angola and Namibia. The interplay between the equatorward trade winds, the Coriolis force, and the presence of the continental boundary leads to the offshore transport of surface waters. As such, this causes coastal upwelling of nutrient-rich South Atlantic Central Water (formed in the western South Atlantic; Stramma and England, 1999) and Antarctic Intermediate Water (AAIW). The upwelled waters are transported equatorward along the coast of Africa via the Benguela Current (BC), giving rise to high biological productivity. Filaments of productive waters can be seen extending from the African continent (Fig. 2). Finally, the Walvis Ridge potentially plays a role in affecting local hydrography and hence the position of the upwelling (Peterson and Stramma, 1991).

The BC, with its two main branches, the Benguela Oceanic Current and the Benguela Coastal Current, is the major northward-flowing component of the BUS which joins the poleward-flowing Angola Current in the north (Stramma and England, 1999). This convergence zone is located between 15 and 18° S and is known as the Angola–Benguela frontal zone. The upwelling zone is bounded by warm current systems, the Angola Current system in the north and the Agulhas Current system in the south (Shannon and Nelson, 1996;
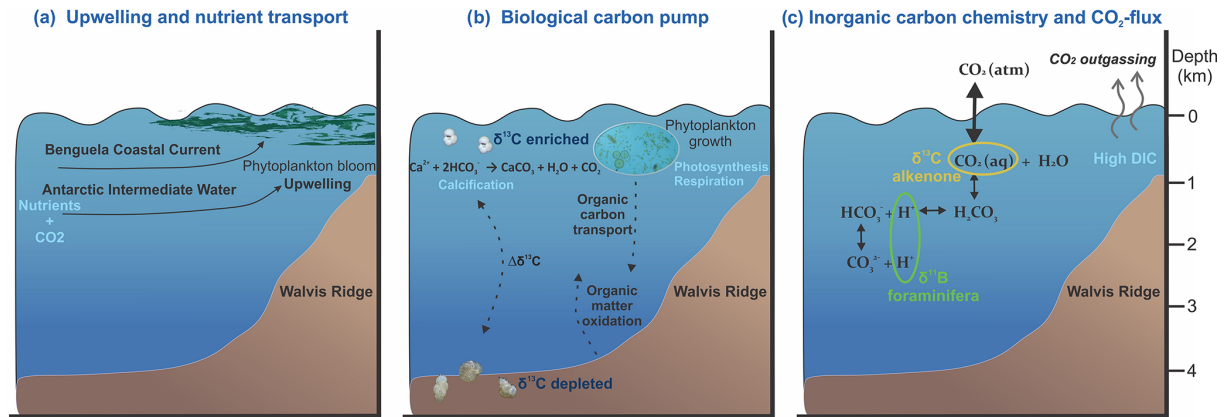
Figure 1. Cross-sections of the Benguela Upwelling System depicting the characteristics of an upwelling region, where **(a)** nutrient- and CO_2-rich waters are upwelled to the surface, **(b)** high productivity contributes to the drawdown of CO_2 in the surface layers via the biological carbon pump, and **(c)** the upwelling strength and efficiency of the biological carbon pump determine variations in the marine inorganic carbon chemistry and hence CO_2 flux.
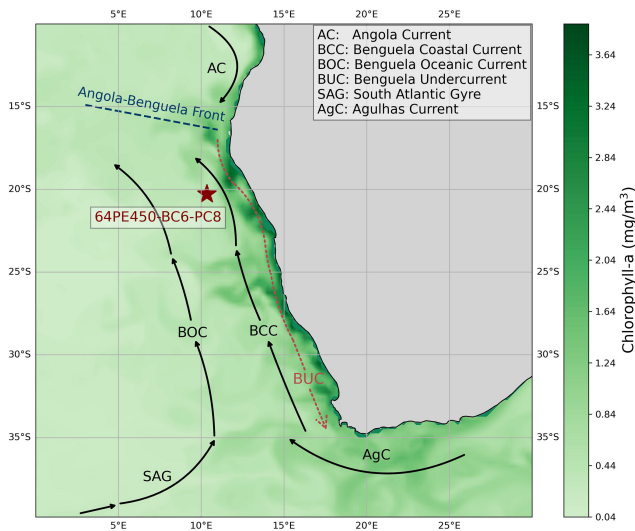
Figure 2. Map showing the location of sediment core 64PE450-BC6-PC8 and the dominant currents shaping the characteristics of the Benguela Upwelling System. The map is overlain with the distribution of surface water chlorophyll-*a* concentration of July 2023 obtained from Global Ocean Biogeochemistry Analysis and Forecast (EU Copernicus Marine Service information; https://doi.org/10.48670/moi-00015, Global Ocean Biogeochemistry Analysis and Forecast, 2024). High chlorophyll-*a* concentrations indicate the high productivity and nutrient-rich upwelled waters of this region today.

Shillington, 1998; Shannon and O'Toole, 2003). Hence, the BC is composed of a mixture of waters originating not only from the mid-latitude surface waters of the central South Atlantic Ocean and the Southern Ocean but also from the Indian Ocean (Gordon, 1986; Lutjeharms and Valentine, 1987). This creates a north-to-south decrease in surface water temperature and salinity in the region (Santana-Casiano et al.,

2009). Hydrographic changes in the region over glacial cycles have been related to changes in the transfer of Indian Ocean waters through Agulhas leakage variability (Knorr and Lohmann, 2003; Peeters et al., 2004; Scussolini and Peeters, 2013).

The BUS region is characterized by year-round upwelling of varying intensity due to the seasonal shift in the South Atlantic gyre. This results in stronger upwelling intensities in June–August compared to the rest of the year (Santana-Casiano et al., 2009; Kämpf and Chapman, 2016). The spatial and temporal dynamics of the BUS result in large variability in the associated CO_2 flux. Predominantly, the surface waters within the BUS act as a CO_2 source (Laruelle et al., 2014; Brady et al., 2019; Roobaert et al., 2019), but this may be interrupted by periods during which they act as a CO_2 sink due to the high primary productivity (Gruber et al., 2009; Gregor and Monteiro, 2013).

3 Proxy interpretation

Reconstruction of inorganic carbon chemistry can be used to constrain past changes in the CO_2 flux between the ocean and atmosphere. Reconstruction of the complete inorganic carbon system is based on at least two parameters of this system (pCO_2, $[CO_3^{2-}]$, $[HCO_3^-]$, pH, [DIC], and total alkalinity) and on the knowledge of temperature and salinity (Zeebe and Wolf-Gladrow, 2001). Commonly used tracers for constraining parameters of the marine inorganic carbon chemistry are based on both organic (e.g., $\delta^{13}C$ of alkenones; Pagani et al., 2002; Pagani, 2014; Popp et al., 1998; Laws et al., 1995) and inorganic (e.g., $\delta^{11}B$ of foraminifera shells; Hemming and Hanson, 1992; Palmer and Pearson, 2003; Foster and Rae, 2016) proxy signal carriers, although these proxies rarely agree completely for upwelling regions (Seki et al., 2010; Palmer et al., 2010) or in general (Rae et al., 2021).

Proxies for seawater carbon chemistry have specific inherent complications, and their application requires critical assumptions. For instance, previous studies have observed discrepancies between alkenone-based pCO_2 reconstruction and ice core records (Palmer et al., 2010; Andersen et al., 1999; Zhang et al., 2013; Witkowski et al., 2020; Jasper et al., 1994), which could be related to disequilibrium between the sea surface and the atmosphere, especially at dynamic sites like upwelling regions. However, it may also be explained by the process of CO_2 uptake in the algal cell, if passive diffusion is not the only way alkenone producers acquire CO_2 in the cell, as suggested by the traditional framework of this proxy (Bidigare et al., 1997). Alkenone producers do use a carbon-concentrating mechanism (CCM; Stoll et al., 2019; Reinfelder, 2011; Bolton and Stoll, 2013; Badger, 2021), which enables carbon acquisition in the cell through the active pumping of HCO_3^- to the chloroplast during low pCO_2 conditions. Also, pCO_2 reconstructions based on alkenone $\delta^{13}C$ values are subject to uncertainties related to the so-called b factor that expresses the effect of multiple parameters related to the physiology of the alkenone producers (Jasper et al., 1994; Rau et al., 1996; Popp et al., 1998). Application of the b factor for the reconstruction of pCO_2 is much debated (e.g., Wilkes and Pearson, 2019), and an adaptation of CCM by the alkenone producers inevitably hampers the application of the proxy. However, there are examples of alkenone-based pCO_2 reconstructions reliably reproducing glacial–interglacial pCO_2 variability (Palmer et al., 2010; Jasper and Hayes, 1990; Bae et al., 2015), potentially related to specific local conditions. As the b value is best represented by a linear relationship to nutrient availability (Bidigare et al., 1997), we rely on the analysis of the barium-to-calcium ratio (Ba / Ca) in planktonic foraminiferal shells that correlates with seawater Ba concentration; hence we used it as a proxy for seawater $[PO_4^{3-}]$ (Lea and Boyle, 1989; Lea and Boyle, 1990b, a; Hönisch et al., 2011).

4　Materials and methods

Samples were taken from box core 64PE450-BC6 and piston core 64PE450-PC8 retrieved from the southern flank of the Walvis Ridge, both taken at the same location (approximately 20.29° S, 10.35° E) at a water depth of ∼ 1375 m b.s.f. The box core consisted of 40.59 cm of sediment, whereas the piston core collected 1453 cm (cut into 15 sections, of which we dated the first 100 cm). The top of the piston core was missing; hence, we used the BC to supplement the missing top of the PC and obtain a near-continuous record, which we here refer to as 64PE450-BC6-PC8. To align the box core and the piston core, lightness reflectance data ($L*$) were used here as an additional constraint to the radiocarbon dates (Supplement Fig. S1). The detailed reflectance data (63 μm resolution) show an overlap between the two cores. The top 4.24 cm of 64PE450-PC8 (later referred to as the disturbed core-top)

overlaps with approximately 30.14 cm of 64PE450-BC6 (i.e., from 10.45 to 40.59 cm b.s.f.). This suggests severe compression of the top of 64PE450-PC8, likely due to the piston coring, but the overlap can still be used to align the age model of the two cores.

The composite record was sampled with a resolution varying between 2 and 5 cm to optimize coverage of the glacial–interglacial transition. All samples were freeze-dried and subsequently split into sub-samples to obtain lipid biomarkers and foraminifera from the same core depth.

4.1　Foraminiferal sample cleaning

Due to their relatively high abundance in upwelling regions and common use in paleoclimate reconstructions (e.g., Spero and Lea, 1996), we selected specimens of *Globigerina bulloides* for the planktonic-foraminifera-based records. Freeze-dried samples were washed over a 63 μm sieve, dried, and further dry-sieved to separate size fractions of 150–315 and 315–425 μm. Specimens of *G. bulloides* were picked from the latter size fraction for analysis of oxygen and carbon isotopes, minimizing any potential impacts of ontogeny. However, as many more specimens were needed, the smaller size fraction was used for radiocarbon, element / calcium (El / Ca), and boron isotope analysis. The foraminifer's size has been shown to affect boron isotopes of several symbiont-bearing planktonic foraminifera species (e.g., *T. sacculifer*, *G. ruber*, *O. universa*; Hönisch and Hemming, 2004; Henehan et al., 2013; Henehan et al., 2016); hence size fraction need to be minimized to avoid introducing uncertainties related to ontogenetic variability. *G. bulloides* is a symbiont-barren species; therefore, boron isotopes are not affected by pH change in their microenvironments related to the symbionts' physiological processes (i.e., respiration, photosynthesis). However, differences in shell size may correspond to different environmental conditions and, for instance, reflect changes in calcification depth and/or seasons (Jonkers et al., 2013; Osborne et al., 2016). Also, previous studies using *G. bulloides* to reconstruct pH relied on a narrow size fraction when the number of specimens allowed this (Raitzsch et al., 2018; Martinez-Boti et al., 2015). Alternatively, a combination of two or more parameters (e.g., temperature and productivity) may impact shell size, resulting in mixed isotopic signatures within size fractions (Metcalfe et al., 2015). Any size-dependent bias on boron isotopes of (symbiont-barren) foraminifera still needs to be investigated; hence we assume that the data presented here for *G. bulloides* reflect average conditions with respect to depth and seasonal variability. To construct a benthic foraminiferal carbon isotope record, specimens of *Cibicidoides wuellerstorfi* were selected from the 315–425 μm size fraction.

Foraminiferal samples were cleaned prior to the analysis of El / Ca ratios and stable isotopes, following an adapted protocol of Barker et al. (2003). This adapted protocol is as follows: for the analysis of the shells' element concentra-

tions in solution and the boron isotopic composition, specimens were carefully cracked using a scalpel to open up the chambers and release potential clay content from the inside. The samples were subsequently transferred to acid-cleaned 1.5 mL vials (Treff) and rinsed three times with deionized water (Milli-Q) and twice with methanol, followed by another thorough rinse with deionized water, using ultrasonication for each rinsing step. To remove all organic material from the shells, samples were placed in a hot block and oxidized with NH_4OH-buffered 1 % H_2O_2 solution for 45 min at 90 °C. To ensure complete removal of organic material, this step was repeated up to three times based on visual inspection. After the oxidative cleaning, the samples were transferred to new pre-cleaned vials (Treff) and leached with diluted acid (1 mM HNO_3) followed by rinsing the samples three times with deionized water. Because the boron isotope analysis is very sensitive to contamination, two additional leaching steps with 1 % NH_4OH were added, followed by rinsing with deionized water, before the acid leaching. Samples for El / Ca and $\delta^{11}B$ analysis were finally dissolved in 500 µL 0.1 M ultra-grade HNO_3 and in 75–80 µL 0.5 M ultra-grade HNO_3, respectively.

Specimens taken for the analysis of El / Ca ratios with a laser ablation quadrupole inductively coupled plasma mass spectrometer (LA-Q-ICP-MS) and for the measurement of $\delta^{18}O$ and $\delta^{13}C$ were cleaned following the same clay removal and oxidative cleaning step as described above but without cracking the shells before the cleaning steps.

4.2 Radiocarbon analysis

Radiocarbon analysis ($^{14}C/^{12}C$) on 50–100 specimens of well-preserved shells of *G. bulloides* was performed at the Laboratory of Ion Beam Physics, ETH Zürich. The analysis of $^{14}C/^{12}C$ followed the protocol described in Wacker et al. (2013, 2014). Briefly, samples were measured with a gas ion source in a Mini Carbon Dating System (MICADAS; Synal et al., 2007) with an automated method for acid digestion of carbonates (Wacker et al., 2013). Samples were placed in 4.5 mL exetainer vials (Labco Limited®, UK) and purged with a flow of 60 mL min^{-1} of helium for 10 min and subsequently leached with 100 µL 0.02 M ultrapure HCl with an automated syringe to remove adsorbed contaminants. Analysis of the released CO_2 from both the leachate and remaining sample provided confirmation for the near-complete removal of contaminants. The CO_2 released from the leachate was directly transported by helium to a zeolite trap and injected into the ion source for $^{14}C/^{12}C$ analysis. The remaining leached sample was acidified with 100 µL ultrapure H_3PO_4 (85 %) and heated at 60 °C for a minimum of 1 h. The released CO_2 was then injected into the ion source for analysis (Wacker et al., 2014; Fahrni et al., 2013). The difference between the radiocarbon values of the leachate and leached samples was less than 5 %. Radiocarbon determinations are given in the conventional radiocarbon ages and cor-

rected for isotopic fractionation via $^{13}C / ^{12}C$ isotope ratios. Calibration was performed using the Marine20 calibration curve (Heaton et al., 2020) with a local correction to the marine reservoir age (ΔR) of 146 ± 85 ^{14}C years (Dewar et al., 2012). These calculations were computed using the Bayesian age–depth model in the Bacon v2.3 package for the R statistical programming software (Blaauw and Christen, 2011).

4.3 Analysis of stable oxygen and carbon isotopes

Pre-weighed 20–40 µg of the shells of *G. bulloides* were dissolved in orthophosphoric acid and analyzed at 71 °C by a Kiel IV device coupled to a MAT 253 isotope-ratio mass spectrometer (IRMS; Thermo Fisher Scientific®) at the NIOZ. Analyses were calibrated using standard bracketing (NBS-19), and the NIOZ house standard (NFHS-1; Mezger et al., 2016) was used to monitor drift. Accuracy and precision for $\delta^{13}C = 0.814 \pm 0.04$ ‰ and $\delta^{18}O = 1.024 \pm 0.12$ ‰ were calculated across several analytical runs of NFHS-1 ($\pm 1\sigma$ SD, $n = 64$).

4.4 Analysis of foraminiferal element / calcium ratios

Prior to the analysis of the samples in solution, a few planktonic foraminifera specimens were screened for preservation to minimize the possibility of diagenetic overprint affecting the geochemical signature of the shells. For this, the ratios of $^{23}Na / ^{43}Ca$, $^{24}Mg / ^{43}Ca$, $^{25}Mg / ^{43}Ca$, $^{27}Al / ^{43}Ca$, $^{55}Mn / ^{43}Ca$, and $^{88}Sr / ^{43}Ca$ were simultaneously monitored during the ablation of single chambers of *G. bulloides* by a laser ablation quadrupole inductively coupled plasma mass spectrometer (LA-Q-ICP-MS). Laser ablation data were acquired on 60 µm diameter spots with a repetition rate of 4 Hz and a laser energy density of ~ 1 J cm^{-2}. The JCp (*Porites* sp. coral) nano-pellet was used to monitor instrumental drift, and JCt (*Tridacna gigas* giant clam; Okai et al., 2004), MACS-3, and the NIOZ Foraminifera House Standard-2-Nano-Pellet (NFHS-2-NP; Boer et al., 2022) provided further quality control on the measurement. NIST SRM 610 was used as the calibration standard. Data were evaluated as both profiles and shell averages.

Approximately 40–50 specimens of *G. bulloides* were dissolved for solution analyses using a sector field inductively coupled plasma mass spectrometer (SF-ICP-MS; Thermo Fisher Scientific® Element 2). The applied cleaning procedure is based on Barker et al. (2003), as discussed above. A pre-scan of calcium concentrations ([Ca^{2+}]) was performed on an aliquot of 30 µL of the dissolved samples, and, based on those data, all samples were subsequently diluted to match [Ca^{2+}] (100 ppm) for element analyses. Isotopes of ^{25}Mg and ^{138}Ba were measured in low resolution. All samples were measured against four ratio calibration standards (de Villiers et al., 2002) and alternated with 0.1 M HNO_3 in between samples to increase the efficiency of wash-out. All samples are drift-corrected using the NFHS-1 standard (Mezger et al.,

2016) and three additional standards, NFHS-2 (Boer et al., 2022), JCp, and JCt (Okai et al., 2004), to evaluate accuracy and precision of the analytical runs. Uncertainty from the internal precision on the basis of short-term stability is $< 2\%$ for both Mg, and Ba. Samples were analyzed in replicates yielding an uncertainty of $< 0.02\,\text{mmol mol}^{-1}$ for Mg and $< 0.14\,\mu\text{mol mol}^{-1}$ for Ba.

4.5 Micro-distillation and boron isotope analysis

Approximately 150 specimens of *G. bulloides* were cleaned for the analysis of boron isotopes. Boron was separated from the calcium carbonate matrix via the micro-distillation technique (Gaillardet et al., 2001; Wang et al., 2010; Misra et al., 2014). A total of $70\,\mu\text{L}$ of the sample was placed on the lid of a Teflon® fin-legged conical beaker (5 mL) and placed upside down on a hotplate at $100\,°\text{C}$ for 20–24 h. The fin-legged vials were wrapped in aluminum foil to provide a heat gradient for a more efficient separation of boron. Once the micro-distillation was complete, the vials were carefully removed from the hotplate while being turned over and were subsequently left for cooling. Sample residue was removed by putting new lids on the beakers, and each sample was diluted with $0.2\,\text{M HF} + 0.2\,\text{M HNO}_3$ for a pre-scan of the boron concentration ([B]). Based on the results of the pre-scan, a final dilution was made to set [B] at 5 ppb for the analysis of $\delta^{11}\text{B}$.

Analysis of the micro-distilled samples was performed at the NIOZ on a Neptune Plus multi-collector inductively coupled plasma mass spectrometer (MC-ICP-MS; Thermo Fisher Scientific®) equipped with high-performance extraction cones (Jet sample cone and "X" skimmer cone) to maximize sensitivity for boron. Samples were injected using a Savillex® $50\,\mu\text{L min}^{-1}$ C-flow nebulizer and Teflon® Scott-type spray chamber. Beams of ^{10}B and ^{11}B were measured on L3 and H3 Faraday cups equipped with amplifiers using $10^{13}\,\Omega$ resistors (Misra et al., 2014; Lloyd et al., 2018). The instrument was tuned to obtain a stable sensitivity, typically 15–$25\,\text{mV ppb}^{-1}\,\text{B}$.

Solutions of $0.2\,\text{M HF} + 0.2\,\text{M HNO}_3$ were used for rinsing throughout the analytical run between analyses and as a matrix for each sample and standard. The analysis followed the approach of sample–standard bracketing using NIST 951 as a reference standard. All samples and quality control standards were analyzed in duplicates; thus average values with $\pm 2\sigma$ standard deviations are reported here. Samples with a replicate precision higher than $\pm 0.6\%\!o$ (2σ) were excluded from this study. A coral standard (Chanakya and Misra, 2022) was treated with the complete carbonate cleaning and micro-distillation procedure for each analytical sequence and repeatedly analyzed to monitor long-term precision ($\delta^{11}\text{B} = 24.57 \pm 0.65\%\!o\,2\sigma$, $n = 64$). Additionally, non-micro-distilled AE-121 standard was analyzed within each run for quality control ($\delta^{11}\text{B} = 19.48 \pm 0.33\%\!o\,2\sigma$, $n = 46$).

In addition to the coral standard, the initial test analysis to validate the boron purification method and instrumental accuracy and precision also included repeated measurements of seawater (Southern Ocean, $\delta^{11}\text{B} = 39.72 \pm 0.25\%\!o\,2\sigma$, $n = 5$) and a boron standard (AE-121) mixed with CaCO_3 (trace metal basis, Acros Organics®) to mimic foraminiferal calcium concentrations ($\delta^{11}\text{B} = 19.53 \pm 0.25\%\!o\,2\sigma$, $n = 18$).

4.6 Estimating past salinity and foraminifera-based temperatures, pH, and $p\text{CO}_2$

Sea surface temperatures (SSTs) were calculated from foraminiferal Mg / Ca values using the species-specific temperature calibration of Mashiotta et al. (1999),

$$\text{Mg} / \text{Ca} = 0.47(\pm 0.03) \times e^{0.107(\pm 0.003) \times \text{SST}}, \qquad (1)$$

where propagated error was calculated based on 1 standard deviation of the duplicate analysis of Mg / Ca and the uncertainty derived from the calibration equation. Mg / Ca values of planktonic foraminifera are known to be affected by salinity and pH changes as well (Gray et al., 2018; Dueñas-Bohórquez et al., 2009; Gray and Evans, 2019); however, a correction for these effects requires independent estimates for salinity and pH with species-specific calibrations. For calculating past carbon chemistry, salinity is an important parameter, and it was estimated based on its conservative relationship with relative sea level change (Waelbroeck et al., 2002). Modern seawater salinity of the BUS (35.43 ± 0.30) was derived from the WOCE Global Data Version 3.0 (Schlitzer, 2000) based on the five closest data points to the location of core 64PE450-BC6-PC8. Using these salinity estimates, the effect of salinity on Mg / Ca-based SST was evaluated and found to have only a small offset in SST values ($< 0.4\,°\text{C}$). As the effect of salinity is relatively minor and adding it would also introduce additional uncertainties, we decided here to refrain from correcting for salinity and pH when calculating past temperatures.

The measured $\delta^{11}\text{B}$ values of *G. bulloides* were converted into pH (Hemming and Hanson, 1992) using Eq. (2):

$$\text{pH} = pK_B^* - \log(-(\delta^{11}B_{\text{sw}} - \delta^{11}B_{\text{borate}})/$$
$$(\delta^{11}B_{\text{sw}} - \alpha \times \delta^{11}B_{\text{borate}} - \varepsilon)), \qquad (2)$$

where the equilibrium constant, pK_B^* (Dickson, 1990), was calculated for each sample based on SST derived from the Mg / Ca values of *G. bulloides* and salinity based on sea level. The fractionation factor between B(OH)_3 and B(OH)_4^-, expressed here as α, is 1.0272 ± 0.0006, from which fractionation, ε, is derived as 27.2 ± 0.6 (Klochko et al., 2006). The boron isotopic composition of seawater, $\delta^{11}B_{\text{sw}}$, is $39.61 \pm 0.2\%\!o$, based on a large range of temperature, salinity, and depth conditions (Foster et al., 2010), and the $\delta^{11}\text{B}$ of borate was calculated from the measured $\delta^{11}\text{B}$ of *G. bulloides* using the species-specific core-top calibration from Raitzsch et al. (2018).

Constraining $p\text{CO}_2$ based on seawater pH requires knowledge of a second independent parameter (Zeebe and Wolf-Gladrow, 2001). For this purpose, total alkalinity was assumed to be the same as today's value at the BUS. Taking the five nearest available data points at the core location from the GLODAPv2023 dataset (Lauvset et al., 2024) defines an average value of $2349 \pm 11 \, \mu\text{mol}\,\text{kg}^{-1}$, which was used to supplement the pH-based $p\text{CO}_2$ reconstruction throughout the 27 kyr record.

Uncertainty on the reconstructed pH value was determined for each sample through error propagation that considered the abovementioned uncertainties of pK_B^*, α, ε, and $\delta^{11}\text{B}_{\text{sw}}$ and the standard deviation (external uncertainty) based on duplicate or triplicate analysis of foraminiferal $\delta^{11}\text{B}$.

Concentrations of CO_2 are based on pH and inorganic carbon chemistry calculations using the PyCO2SYS package (Humphreys et al., 2022) in Python version 3.11.2. Uncertainty is propagated for each computed carbon chemistry parameter as described in Humphreys et al. (2022).

4.7 Lipid extraction and alkenone analyses

Lipids were extracted from the freeze-dried and homogenized sediment samples using an accelerated solvent extractor (ASE® 350, DIONEX®) at the NIOZ. Samples were extracted with dichloromethane (DCM) and methanol (9 : 1, v/v) at 100 °C to obtain the total lipid content and subsequently dried under N_2 gas at 35 °C in a Caliper TurboVap LV Evaporator. Samples were then redissolved in DCM and run through an Na_2SO_4 column to eliminate excess water. The extract was passed through an alumina (Al_2O_3) column and separated into apolar, ketone, and polar fractions using a mixture of hexane : DCM (9 : 1, v/v), hexane : DCM (1 : 1, v/v), and DCM : methanol (1 : 1, v/v), respectively. All extracts were dried under N_2, and the ketone fraction was further utilized to obtain the relative abundance and $\delta^{13}\text{C}$ values of the long-chain alkenones.

Ketone fractions were dissolved in ethyl acetate, and concentrations of alkenones were measured using a gas chromatograph with flame ionization detection (GC-FID; Agilent® 6890N) equipped with a silica capillary column (CP-Sil 5 CB; 50 m × 0.32 mm, 0.12 μm film thickness). The temperature program of the GC-FID analyses used an initial temperature of 70 °C that increased with a rate of 20 °C min^{-1} to 200 °C followed instantly by heating at a rate of 3 °C min^{-1} until it reached 320 °C, where it remained constant for 10 min.

Based on the initial concentration measurement, samples were diluted with ethyl acetate to allow stable carbon isotope analysis using a gas chromatography isotope ratio mass spectrometer (GC-IRMS; Thermo Fisher Scientific® Delta V Advantage Trace® 1310). The GC-IRMS was equipped with cross-bond trifluoropropylmethyl polysiloxane columns (Rtx-200; 60 m × 0.32 mm, 0.5 μm film thickness) and helium as a carrier gas. Each sample was manually injected

onto the GC-IRMS. The starting temperature of the GC-IRMS was 70 °C, which then increased by 18 °C min^{-1} until reaching 250 °C. After reaching that temperature, heating continued with 1.5 °C min^{-1} until 320 °C, where it was kept stable for 25 min. Samples were analyzed for carbon isotopes in duplicates, and instrumental accuracy was monitored through measurement of the B5 n-alkane mixture standard (provided by A. Schimmelmann, Indiana University) every day (i.e., after every 6–7 samples). The IsoLink II combustion reactor was oxidized for 10 min every day before the start of standard and sample analysis. Each analysis was followed by 2 min of seed oxidation to maintain the reactor oxygenation.

4.8 Calculation of alkenone-based temperatures and $p\text{CO}_2$

Alkenone-based sea surface temperatures were derived from the ketone unsaturation index ($\text{U}_{37}^{K'}$), where $\text{U}_{37}^{K'}$ is defined as the relative abundance of di- and tri-unsaturated C_{37} methyl alkenones (Prahl and Wakeham, 1987):

$$\text{U}_{37}^{K'} = \text{C}_{37:2}/(\text{C}_{37:3} + \text{C}_{37:2}). \tag{3}$$

Sea surface temperature was then calculated using the alkenone temperature calibration model developed for the Atlantic region (Conte et al., 2006).

Fractionation of stable carbon isotopes during photosynthesis ($\varepsilon_{p37:2}$) can be computed based on the difference between the carbon isotopic ratio of aqueous carbon dioxide ($\delta^{13}\text{C}_{\text{CO}_2}$) and the organic biomass ($\delta^{13}\text{C}_{\text{org}}$):

$$\varepsilon_{p37:2} = [(\delta^{13}\text{C}_{\text{CO}_2}+1000)/(\delta^{13}\text{C}_{\text{org}}+1000)-1]\times 1000. \tag{4}$$

$\delta^{13}\text{C}_{\text{CO}_2}$ was derived from the carbon isotopes of planktonic foraminifera, *G. bulloides*, corrected for the temperature-dependent fractionation during calcite precipitation (Romanek et al., 1992) and the fractionation between dissolved and gaseous carbon dioxide (Mook et al., 1974).

$\delta^{13}\text{C}_{\text{org}}$ was calculated from the carbon isotopes of di-unsaturated alkenones ($\delta^{13}\text{C}_{37:2}$) as

$$\delta^{13}\text{C}_{\text{org}} = [(\delta^{13}\text{C}_{37:2} + 1000) \times (\Delta\delta^{13}\text{C}_{\text{org}} + 1)] - 1000, \tag{5}$$

where $\Delta\delta^{13}\text{C}_{\text{org}}$ expresses the carbon isotopic difference between $\text{C}_{37:2}$ and DIC, which has been defined between 3‰– 6‰ based on culture experiments (Riebesell et al., 2000; Schouten et al., 1998; van Dongen et al., 2002). Here, we take the commonly applied value of 4.2‰ (Bijl et al., 2010; Pagani et al., 2005; Pagani et al., 2010; Pagani et al., 2011; Seki et al., 2010; Palmer et al., 2010).

Based on $\varepsilon_{p37:2}$, aqueous CO_2 ($[\text{CO}_2]_{\text{aq}}$) can be reconstructed as follows (Hayes, 1993; Pagani et al., 2002):

$$[\text{CO}_2]_{\text{aq}} = b/(\varepsilon_{\text{f}} - \varepsilon_{p37:2}), \tag{6}$$

where ε_{f} stands for the carbon isotopic fractionation associated with carbon fixation estimated as 25‰ (e.g., Popp et al.,

1998). Parameter b expresses all physiological factors affecting total carbon isotope fractionation, including cell shape and size, membrane permeability, and the algae's growth rate (Jasper et al., 1994; Rau et al., 1996; Popp et al., 1998; Conte et al., 1994; Riebesell et al., 2000). Earlier studies using phytane (Bice et al., 2006; Damsté et al., 2008) and alkenone (Witkowski et al., 2018) to reconstruct $p\mathrm{CO_2}$ estimated b for a mean value of $165\,‰–170\,‰\,\mathrm{kg}\,\mu\mathrm{M}^{-1}$. As growth rate and thereby nutrient availability have a large influence on the physiological factors and, accordingly, b values are highly correlated to $[\mathrm{PO_4^{3-}}]$ (Bidigare et al., 1997), b can be best described at our core site by estimating past changes in $[\mathrm{PO_4^{3-}}]$ (Pagani et al., 2005). Here, $[\mathrm{PO_4^{3-}}]$ is estimated based on the Ba/Ca ratio of planktonic foraminifera, *G. bulloides* (Lea and Boyle, 1989; Lea and Boyle, 1990b, a; Martin and Lea, 1998; Lea and Boyle, 1991). We therefore constrain past changes in b as (Pagani et al., 2005)

$$b = [118.52 \times (\mathrm{Ba/Ca} \times [\mathrm{PO_4^{3-}}]_{\mathrm{modern}}/\mathrm{Ba/Ca}_{\mathrm{modern}}) + 84.07]. \tag{7}$$

Average modern $\mathrm{PO_4^{3-}}$ concentration ($[\mathrm{PO_4^{3-}}]_{\mathrm{modern}}$) in the BUS is $0.63\,\mu\mathrm{mol}\,\mathrm{kg}^{-1}$ (obtained from GLODAPv2023; Lauvset et al., 2024; Olsen et al., 2016; Key et al., 2015), whereas the corresponding modern foraminiferal Ba/Ca value ($\mathrm{Ba/Ca}_{\mathrm{modern}}$) was analyzed here ($19.08\,\mu\mathrm{mol}\,\mathrm{mol}^{-1}$). Equation (7) basically assumes a constant and proportional relation between Ba and $[\mathrm{PO_4^{3-}}]$. This seems reasonable for our purposes, as surface water Ba concentration has been shown to be reflected proportionally in foraminiferal Ba/Ca (Lea and Boyle, 1991; Hönisch et al., 2011) and the cold nutrient-rich surface waters are generally enriched in dissolved barium (e.g., Davis et al., 2020).

To calculate atmospheric $p\mathrm{CO_2}$ from aqueous concentrations of $\mathrm{CO_2}$, Henry's law was applied using the temperature- and salinity-dependent solubility constant, K_0.

$$p\mathrm{CO_2} = [\mathrm{CO_2}]_{\mathrm{aq}}/K_0 \tag{8}$$

Uncertainty propagation for the calculated $p\mathrm{CO_2}$ values was based on the errors derived from 1 standard deviation of duplicate analysis of $\delta^{13}\mathrm{C}$ of the extracted ketone fraction, $\delta^{13}\mathrm{C}$ of foraminifera, and Ba/Ca values of foraminifera. The largest uncertainty in alkenone-based $p\mathrm{CO_2}$ reconstructions originates from the estimated past $[\mathrm{PO_4^{3-}}]$, and, to incorporate potential variation in nutrient levels during the deglaciation, an additional uncertainty of $0.2\,\mu\mathrm{mol}\,\mathrm{kg}^{-1}$ was assigned to the known modern values of $[\mathrm{PO_4^{3-}}]$. This uncertainty is based on the gradient measured today in the upper $50\,\mathrm{m}$ of the water column, which is more than the variability observed in surface water today but also includes potential changes in the upwelled waters.

5 Results

5.1 Radiocarbon ages

The calibrated mean radiocarbon ages generally increase with depth in both BC and PC cores used here. Sediment core 64PE450-BC6 comprises 40.59 cm, where the core-top sample was dated at 4.863 ka, and an age of 9.551 ka at 40 cm b.s.f. (Fig. 3a). This suggests an average sedimentation rate of about $10\,\mathrm{cm}\,\mathrm{kyr}^{-1}$, with somewhat higher values ($> 10\,\mathrm{cm}\,\mathrm{kyr}^{-1}$) in the top 12 cm. Radiocarbon dates at the top of the box core (0–11 cm) indicate reversed ages (4.9 ka at 11 cm and 5.2 ka at 1 cm uncalibrated ages). This interval also corresponds to elevated Ca / Al, Ti / Al, and Si / Al ratios measured through X-ray fluorescence (XRF) core scanning (Fig. S2; using the method described in Weltje and Tjallingii, 2008). The enrichment of elements commonly found in coarse fractions and heavy minerals is likely due to the removal of fine-fraction material by winnowing, which may have also contributed to the loss of the last 4.8 kyr in the sedimentary record. Alternatively, the upper 10 cm b.s.f. has constant ages due to bioturbation. Radiocarbon analyses from sediment core 64PE450-PC8 included six samples of the upper 100 cm of sediment collected. The age–depth model for this core suggests 9.994 ka at 5 cm b.s.f. depth (Fig. 3b) and indicates the presence of a disturbed core-top. Low sedimentation rates ($2\,\mathrm{cm}\,\mathrm{kyr}^{-1}$) characterize the top 10 cm b.s.f. of this core, which is approximately in line with the sedimentation rate in the deepest parts of box core 64PE450-BC6 ($\sim 6\,\mathrm{cm}\,\mathrm{kyr}^{-1}$). However, the average sedimentation rate in 64PE450-PC8 is lower ($4\,\mathrm{cm}\,\mathrm{kyr}^{-1}$) compared to the average values observed in the box core, which, in part, might also be due to compaction with increasing depth. The top 60 cm b.s.f. of the core shows a steady increase in sedimentation rate ($2–7\,\mathrm{cm}\,\mathrm{kyr}^{-1}$); therefore the low average values may be attributed to a relatively abrupt decrease in sedimentation rate at 60 cm b.s.f. in the core, which corresponds to an age of 23.586 ka. Between 60 and 100 cm b.s.f. depth, sedimentation rates remain 1–$2\,\mathrm{cm}\,\mathrm{kyr}^{-1}$. Due to the uncertainty related to sediment deposition between 60 and 100 cm b.s.f. of the piston core, this study focuses only on the 40.59 cm b.s.f. of core 64PE450-BC6 and the upper 65.5 cm b.s.f. of core 64PE450-PC8.

5.2 Stable isotopes

Carbon isotope values of the planktonic foraminifer, *G. bulloides*, vary between $-1.4\,‰$ and $0.6\,‰$ (VPDB). The glacial part of the record is marked by relatively high $\delta^{13}\mathrm{C}$ values with a maximum of $0.6\,‰$ at 23.3 ka. After that, there is a rapid decrease to a value of $-1.1\,‰$ at 22 ka, followed by a period of varying $\delta^{13}\mathrm{C}$ values between $-0.6\,‰$ and $0.1\,‰$ until 18 ka. Between 18 and 16 ka, $\delta^{13}\mathrm{C}$ values decrease to a minimum value of $-1.4\,‰$, and then, with a slight increase, values stabilize around $-1.1\,‰$ until 11 ka. Dur-
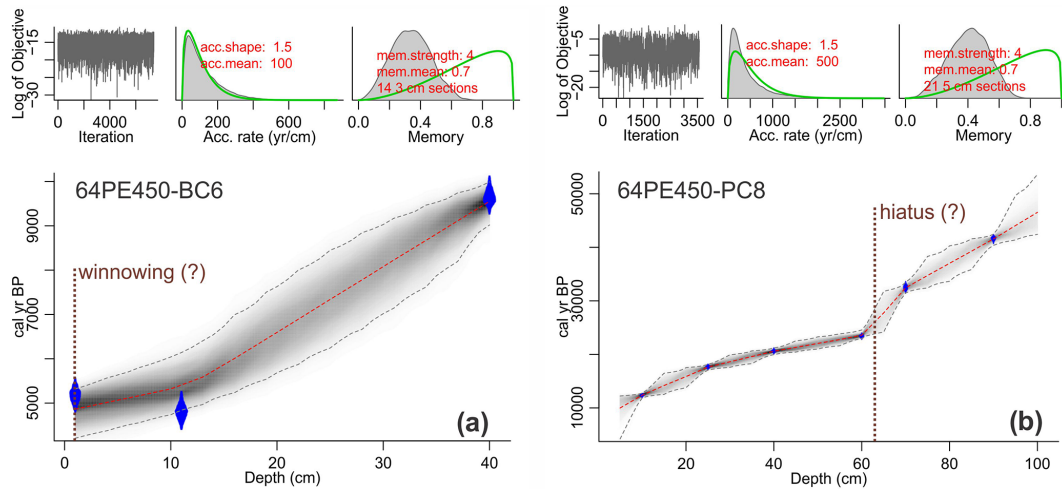
Figure 3. Age–depth model of **(a)** 64PE450-BC6 (box core) and **(b)** 64PE450-PC8 (piston core) based on radiocarbon dates, where blue diamonds indicate the sampling depth for ^{14}C analysis. The calibration of radiocarbon ages and the figure was generated using the Bacon v2.3 package for the R statistical programming software (Blaauw and Christen, 2011). Calibration was performed using the Marine20 calibration curve (Heaton et al., 2020) with a local carbon reservoir correction (ΔR) of 146 ± 85 ^{14}C years (Dewar et al., 2012). Dashed red lines show mean values of the best-fitted model, and dashed gray lines indicate the 95 % confidence interval. Note that, due to the disturbed core-top and potential hiatus in the piston core as indicated in panel **(b)**, only the interval from 4.25 to 65.5 cm of 64PE450-PC8 was used for temperature and carbon system reconstruction in this study.
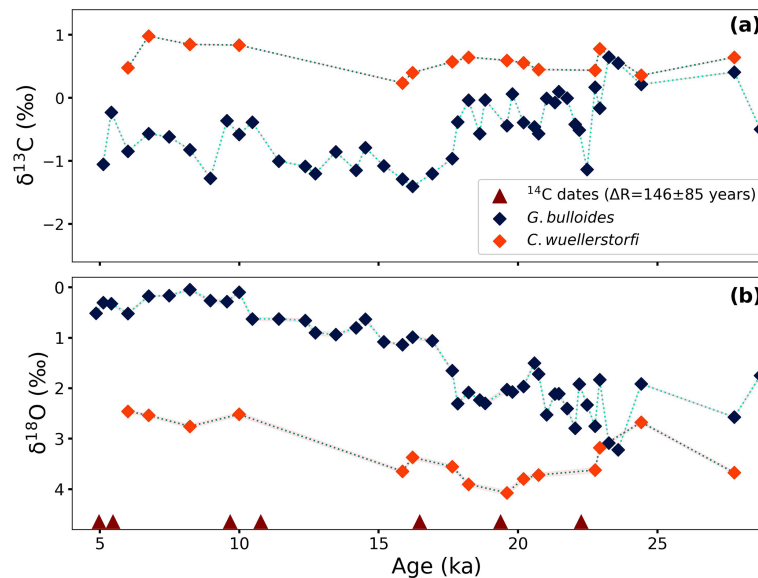
Figure 4. (a) δ^{13}C and **(b)** δ^{18}O values of planktonic (*G. bulloides*) and benthic (*C. wuellerstorfi*) foraminifera plotted with the age model. Red triangles indicate the ages tied with radiocarbon dates.

ing the Holocene, δ^{13}C values of *G. bulloides* vary between -1.3‰ and -0.2‰ (Fig. 4a). The δ^{13}C values of the benthic foraminifer, *C. wuellerstorfi*, although measured at somewhat lower resolution, range between 0.5‰ and 1.0‰. It appears that benthic δ^{13}C values were on average 0.2‰ heavier during the Holocene compared to the glacial (Fig. 4a).

The δ^{18}O values of *G. bulloides* range from 0.0‰ (VPDB) to 3.2‰ with the most depleted values at ~ 8 ka (Fig. 4b).

The highest values of δ^{18}O can be seen at 23.6 ka (peak glacial), after which values show rapid changes and subsequently continue to decrease gradually before reaching a plateau at about 10 ka. During the Holocene, these values stayed relatively stable and varied only between 0.0‰ and 0.6‰ (VPDB). The trend differs from the lower-resolution benthic record of δ^{18}O measured on *C. wuellerstorfi* (Fig. 4b). The benthic foraminiferal δ^{18}O values are

consistently higher compared to the *G. bulloides* values, which is in line with lower bottom-water temperatures. This difference, however, appears smaller during the end glacial than during the Holocene.

The boron isotopic composition of the planktonic foraminifer, *G. bulloides*, ranges between 15.1‰ and 17.0‰ (relative to NIST 951), with larger variations during the last 6–5 kyr (Fig. 5a). The lowest $\delta^{11}B$ values were observed at 5.4 ka, whereas $\delta^{11}B$ values reach a maximum at 13.5 ka. Prior to this maximum value, $\delta^{11}B$ values show an increasing trend from 27.8 to 13.5 ka (Fig. 5a).

The carbon isotopic composition of the alkenones shows its heaviest value ($-22.4‰$) at 19.6 ka. After this peak, $\delta^{13}C$ values reach a minimum ($-23.4‰$) at 15.9 ka then increased again towards the most recent values ($-22.7‰$ to $-22.9‰$; Fig. 5b).

5.3 Element / Ca ratios in the planktonic foraminifer, *G. bulloides*

Mg / Ca reaches maximum values of 2.85 and 2.81 mmol mol^{-1} at 16.9 and 6.7 ka, respectively (Fig. 5c). Substantially lower values characterize the interval between 16.9 and 6.7 ka, when Mg / Ca ranges between 2.46 and 2.69 mmol mol^{-1}. The lowest values (2.30–2.40 mmol mol^{-1}) were found at 4.9–5.4 ka and 21.3–27.8 ka.

The general trend in foraminiferal Ba / Ca shows an increase from glacial to recent (Fig. 5d). The oldest part of the record shows relatively stable Ba / Ca values at around 6 µmol mol^{-1}. During the last 15 kyr, however, more variability is observed for Ba / Ca. The highest Ba / Ca value (19.1 µmol mol^{-1}) is observed at the top of the record, and the lowest values, 4.02 and 3.94 µmol mol^{-1}, are observed at 17.6 and 27.8 ka, respectively.

5.4 $U^{K'}_{37}$ sea surface temperatures

The alkenone-based $U^{K'}_{37}$ record shows a continuous increase throughout the deglaciation (Fig. S3). The lowest value (0.56) was measured at 27.8 ka and increases to 0.58 until 23.6 ka. The interval of 22.0–19.6 ka again records low $U^{K'}_{37}$ values, which then follows a steady increase until 9.6 ka. During the early Holocene, $U^{K'}_{37}$ values stabilize around 0.7 until 6.8 ka, when values slightly start to decrease, reaching 0.67 in the uppermost part of the record.

6 Discussion

6.1 Local temperatures over the Last Glacial Maximum (LGM), last deglaciation, and Holocene

The proxy-based temperature reconstructions resemble the Southern Hemisphere climate responses based on the gradual temperature increase from 23 ka onwards (e.g., Petit et al., 1999; Suggate and Almond, 2005; Clark et al., 2009). However, comparing these reconstructions with both Northern Hemisphere (NGRIP; North Greenland Ice Core Project Members, 2004) and Southern Hemisphere (EPICA-Dome C; EDC; Jouzel et al., 2007) records, it is evident that individual climate events also show similarities to the trends observed in the Northern Hemisphere (Fig. 6). This suggests that the location of 64PE450-BC6-PC8 reflects a complex structure of the water column temperature, potentially affected by both Northern and Southern Hemisphere climatic changes.

The $U^{K'}_{37}$-based sea surface temperature reconstruction shows low temperatures (18.2–18.5 °C) between 23.6 and 18.6 ka (Fig. 6a), which corresponds to the relatively low temperatures in the record based on the $\delta^{18}O$ values from the shells of *G. bulloides*. These temperature minima and the relatively high variability (1.5‰–3.2‰) shown by the $\delta^{18}O$ record between 24 and 21 ka indicate the Last Glacial Maximum (LGM; e.g., Clark et al., 2009; Hughes et al., 2013) within this record. While the trends observed here are in agreement with the general deglacial temperature records from higher latitudes, such a pattern is not reflected by the temperature record based on Mg / Ca ratios of *G. bulloides*. In fact, the Mg / Ca-based temperature trend is only between 23 and 16 ka comparable to the other local ($U^{K'}_{37}$, foraminifera $\delta^{18}O$) and high-latitude reconstructions (ice core $\delta^{18}O$; e.g., Jouzel et al., 2007), after which this trend deviates from the classic deglacial pattern showing decreasing temperatures towards the Holocene.

While all these proxies have their inherent complications, the discrepancies between these records likely also reflect changes in the interaction between the core site and the higher latitudes. For instance, foraminiferal $\delta^{18}O$ values not only depend on temperature, but also on the stable oxygen isotopic signature of the water and hence salinity. This may result in a signal of increasing temperatures in the $U^{K'}_{37}$ and Mg / Ca records, but not in the $\delta^{18}O$ record (e.g., between 20 to 18 ka), due to a change in salinity that may compensate the impact of warming on $\delta^{18}O$ values. Shifts in river runoff, for example, might also have impacted local seawater $\delta^{18}O$ and hence foraminiferal oxygen isotopes. Similarly, multiple studies suggested an overall reduced Agulhas leakage during the LGM compared to deglacial levels (Pether, 1994; Flores et al., 1999; Rau et al., 2002; Peeters et al., 2004; Charles and Morley, 1988; Wefer et al., 1996; Franzese et al., 2006), and changes therein could also have resulted in enhanced $\delta^{18}O$ variability during the LGM.

Not only the trends but also absolute values differ between the temperature reconstructions (i.e., $U^{K'}_{37}$ and Mg / Ca), which likely reflects a difference in water depth where the proxy signal carriers lived. Alkenone-based temperature reconstruction agrees with reported modern SSTs from the upper 50 m of the northern Benguela (Santana-Casiano et al., 2009), while the foraminifer-based temperature (Mg / Ca) corresponds to the values observed somewhat deeper (100–
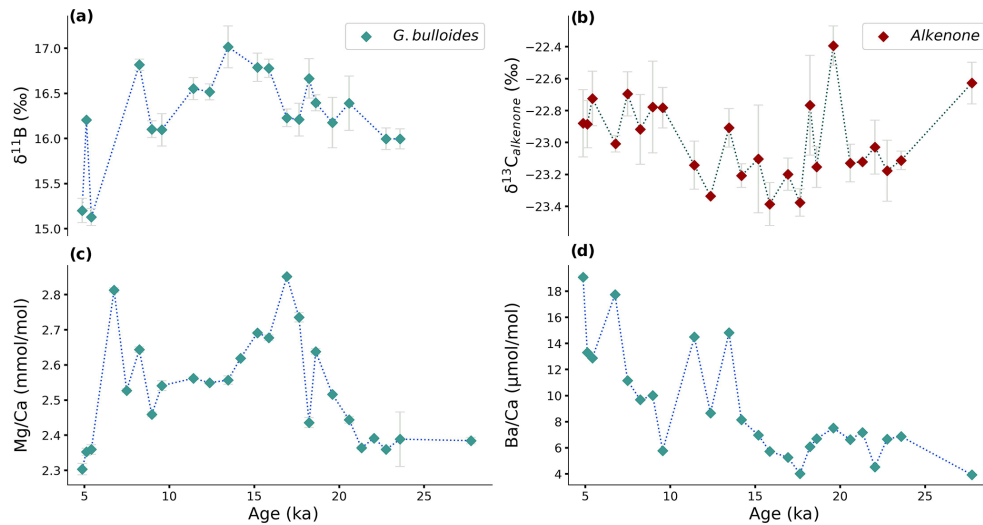
Figure 5. Measured **(a)** foraminiferal δ^{11}B, **(b)** alkenone δ^{13}C, and foraminiferal element concentrations **(c)** Mg / Ca **(d)** Ba / Ca plotted over the past 27.8 kyr at the Benguela Upwelling System. Error bars show $\pm\,1\sigma$ standard deviation. When error bars are not shown, the error of the duplicate measurement is smaller than the symbol.

150 m; GLODAPv2023; Lauvset et al., 2024; Fig. S4). The vertical dispersion of *G. bulloides* may be large, but the 100–150 m living habitat corresponds well with previously reported living depths for this species (Tapia et al., 2022; Lessa et al., 2020; Rebotim et al., 2017). The offset between $U^{K'}_{37}$ and foraminiferal Mg / Ca values during the LGM is about 3.0 °C, and this gradually increases to 5.6 °C during the early Holocene. This implies that foraminiferal Mg / Ca values are affected by other factors than local SST alone. Partial dissolution of foraminiferal shells at depth may affect Mg / Ca values and thereby bias reconstructed temperatures through the preferential loss of Mg^{2+} (Dekens et al., 2002; Regenberg et al., 2006). However, the impact of dissolution is probably minor only because the water depth at site 64PE450-PC8-BC6 is less than 1.4 km and *G. bulloides* is reported to be less sensitive to dissolution compared to other surface dwellers (Mekik et al., 2007). While Mg / Ca values may also be affected by early diagenesis (Hover et al., 2001; Kozdon et al., 2013; Ni et al., 2020; Panieri et al., 2017; Sexton et al., 2006; Stainbank et al., 2020), El / Ca ratios in the shell's profile obtained through laser ablation did not show any evidence for such diagenetic effects.

Inconsistent trends and minor changes in absolute temperature values over the last 27 kyr in this record make it challenging to identify millennial-scale climate events with confidence. The last deglacial was marked by large climate fluctuations primarily linked to the release of meltwater in the Northern Hemisphere weakening Atlantic Meridional Overturning Circulation (AMOC; McManus et al., 2004; Rahmstorf, 2002; Denton et al., 2010; Hodell et al., 2017; Pöppelmeier et al., 2023). This, in turn, changed global heat distribution causing cooling in the North Atlantic region that may have been accompanied by warming in the

Southern Hemisphere (Broecker, 1998; Stocker, 1998). Such well-known climate events include Heinrich Stadial 1 (HS1; $\sim$ 17.8–14.5 ka; e.g., Bond et al., 1993; Cacho et al., 1999; McManus et al., 1994; Calvo et al., 2007; Wang et al., 2013) and the Younger Dryas (YD; $\sim$ 12.8–11.6 ka; Rühlemann et al., 1999; Kaplan et al., 2010; Panmei et al., 2017; Blunier and Brook, 2001; Alley, 2000), which were interrupted by a warming known as the Bølling–Allerød (B–A) Northern Hemisphere warming ($\sim$ 14.6–12.9 ka; e.g., Pedro et al., 2016; Blunier et al., 1997; Lamy et al., 2007; Vandergoes et al., 2008). While high-latitude Southern Hemisphere records present warming signals during HS1 and YD, our temperature records remain relatively constant at the time of these events, and only the alkenone-based temperatures indicate slight warming at 12.4–11.4 ka. Deviating trends shown by the different proxy signal carriers are evident at the time of the B–A Northern Hemisphere warming, when Southern Hemisphere temperature reconstructions are also inconsistent at other locations (Lamy et al., 2007; Vandergoes et al., 2008).

Comparing the trends observed in the different proxies points to the dynamic glacial–deglacial history of the BUS, which was likely shaped by a varying influence of southern- and northern-sourced waters. Also, minor offsets might be explained by changes in either seasonality between haptophytes and *G. bulloides* (Leduc et al., 2010) or differences in water depth where the signals were recorded. Hence, such differences between the records could be due to a shift in productive season and/or a shift in depth habitat. As unraveling these signals is highly speculative, we focus on the glacial vs. interglacial contrasts observed.
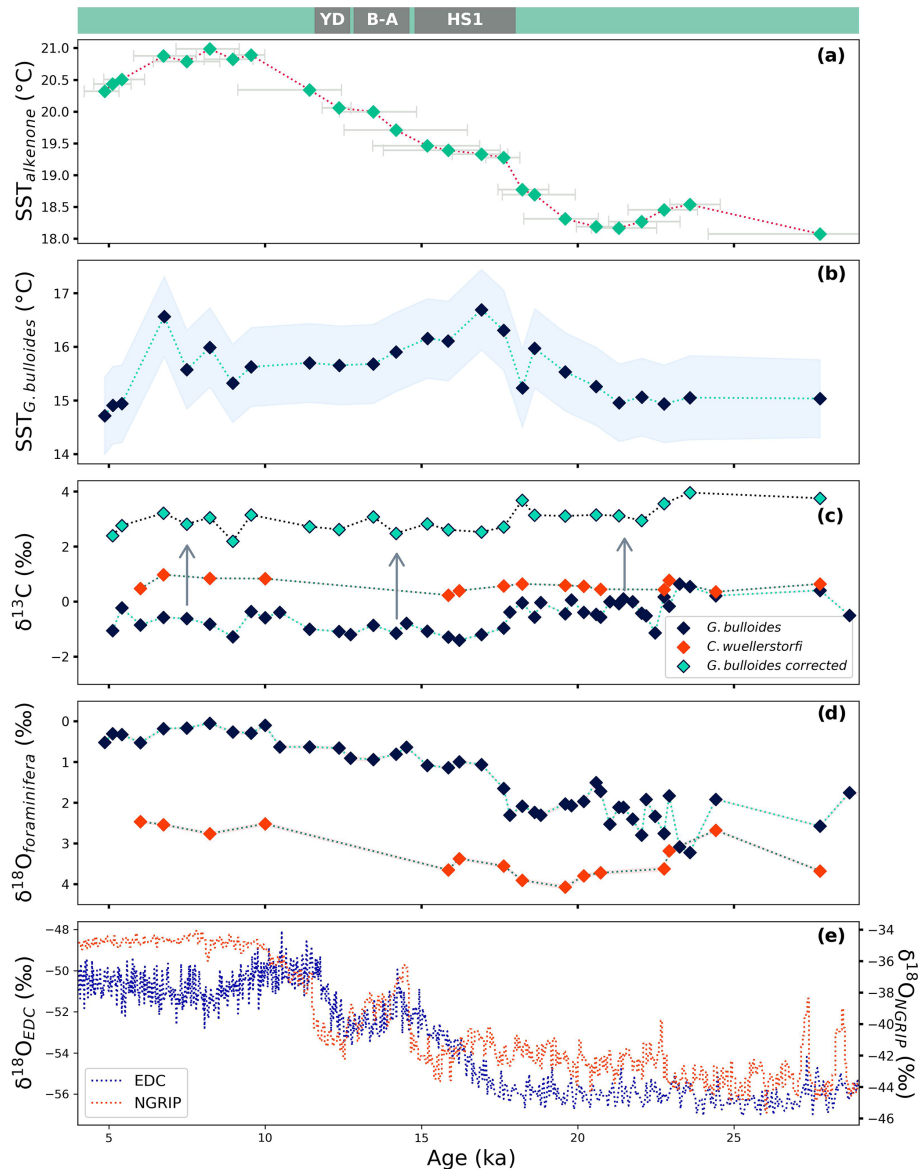
Figure 6. Reconstructed sea surface temperatures (SSTs) based on **(a)** the alkenone unsaturation index, $U_{37}^{K'}$, and **(b)** foraminiferal Mg / Ca; **(c)** δ^{13}C analyzed in benthic (*C. wuellerstorfi*) and planktonic (*G. bulloides*) foraminifera with corrected values; **(d)** δ^{18}O of benthic (*C. wuellerstorfi*) and planktonic (*G. bulloides*) foraminifera; and **(e)** the δ^{18}O ice core record from EPICA Dome C (EDC; Jouzel et al., 2007) and the North Greenland Ice Core Project (NGRIP; North Greenland Ice Core Project Members, 2004) shown for the past 29 kyr. Corrected δ^{13}C values of *G. bulloides* marked with green diamonds in panel **(c)** are based on temperature (derived from Mg / Ca ratios; Bemis et al., 2000) and $[CO_3^{2-}]$ values (derived from pH and TA; Bijma et al., 1999), and arrows indicate the direction of the correction. The modern-day SST at core site 64PE450-BC6-PC8 is approximately 20.7 °C (GLODAPv2023; Lauvset et al., 2024; Santana-Casiano et al., 2009). Major climate events (YD: Younger Dryas; B–A: Bølling–Allerød interval; HS1: Heinrich Stadial 1) are marked above the top panel as reference. Horizontal error bars in panel **(a)** show the age uncertainty based on the 95 % confidence interval of the calibrated age. The shaded blue area in panel **(b)** indicates the error propagated from temperature calibration uncertainty and the ± 1σ standard deviation of the duplicate measurement of the samples. Analysis of the stable isotopes **(c, d)** provided an error smaller than the symbols shown in the figure.

6.2 Biological carbon pump

Comparing benthic (*C. wuellerstorfi*) and planktonic (*G. bulloides*) trends in δ^{13}C shows they have similar values during the last glacial and higher δ^{13}C values for the benthic than for the planktonic foraminifera during the interglacial. This is in contrast to what would be expected if BCP determined the foraminiferal carbon isotope signatures (Hain et al., 2014; Hilting et al., 2008). Generally, DIC in surface waters is enriched in ^{13}C, as the BCP results in preferential

export of ^{12}C-rich organic matter to the deeper water masses, where it is released through remineralization. The efficiency and strength of the BCP is known to be affected by multiple processes, such as the formation, sinking, and interaction of aggregates with other minerals (Fowler and Knauer, 1986; Alldredge and Silver, 1988; Armstrong et al., 2001; Francois et al., 2002; Klaas and Archer, 2002; De La Rocha and Passow, 2007; Turner, 2015), and the efficiency is generally reflected by the offset in ^{13}C between the surface and deep water ($\Delta\delta^{13}$C). However, species-specific offsets from equilibrium values between seawater DIC δ^{13}C and foraminiferal carbonate δ^{13}C can challenge interpretation of the $\Delta\delta^{13}$C and are likely responsible for the lower δ^{13}C values of *G. bulloides* compared to *C. wuellerstorfi* observed here.

Application of foraminiferal $\Delta\delta^{13}$C as their proxy for BCP efficiency requires a direct relation with the δ^{13}C of DIC. Benthic foraminiferal δ^{13}C values, and, in particular δ^{13}C values of the epifaunal *C. wuellerstorfi*, are generally considered faithful recorders of the δ^{13}C values of DIC, with carbonate δ^{13}C values being close to equilibrium (Thomas and Shackleton, 1996; Hilting et al., 2008). The stable carbon isotopic composition of DIC today is approximately 0.5‰–0.7‰ at a depth of 1.3 km along the latitude 20° S (Kroopnick, 1980; Kroopnick, 1985; Sarnthein et al., 1994; Curry and Oppo, 2005; Schmittner et al., 2013), which agrees well with the value inferred from *C. wuellerstorfi* in the uppermost sample (6.0 ka) of core 64PE450-BC6-PC8.

Stable carbon isotopic values from planktonic foraminifera have been shown to be generally lower with respect to the equilibrium values of DIC (Kahn, 1979; Kahn and Williams, 1981; Oppo and Fairbanks, 1989; Spero, 1992), indicating a strong biological impact (i.e., the vital effect; e.g., Spero, 1992; de Nooijer et al., 2014; Erez, 2003). For instance, symbiont-bearing species such as *O. universa* and *T. sacculifer* show offsets in δ^{13}C as much as 1.8 and 1.4‰, respectively, depending on irradiance level (Spero, 1992; Spero and Lea, 1993). Although *G. bulloides* lacks algal symbionts (Hemleben et al., 1989), it has been shown to deviate even more from the ambient seawater δ^{13}C values (Kahn and Williams, 1981; Spero and Lea, 1996). Several factors likely add together to the observed offset, such as carbon chemistry ($[CO_3^{2-}]$; Spero et al., 1997; Bijma et al., 1999), temperature (Bemis et al., 2000), and respiration (Zeebe et al., 1999). The range of $[CO_3^{2-}]$ and temperature observed within our 27 kyr record may yield a δ^{13}C offset of 0.6‰–1.4‰ and 2.4‰–2.6‰, respectively. More recently, Bird et al. (2017) suggested that bacterial symbiosis may also partly explain the observed offset for δ^{13}C in *G. bulloides*. While symbiont photosynthesis contributes to elevating foraminiferal δ^{13}C due to preferential ^{12}C removal, the geochemical signature of *G. bulloides* is more likely to be controlled by the respiration of photoautotrophic cyanobacteria that produce depleted CO_2 and hence decrease shell δ^{13}C values (Bird et al., 2017). Irrespective of the process involved, a substantial correction

has to be applied to the δ^{13}C values of *G. bulloides* to approach the heavier seawater DIC δ^{13}C values. Increasing temperature (Bemis et al., 2000) and $[CO_3^{2-}]$ (Bijma et al., 1999) will also increase the offset between δ^{13}C values of *G. bulloides* and seawater [DIC], suggesting that larger corrections are required during the Holocene than during the last glacial. Still, when the corrections for changes in temperature and $[CO_3^{2-}]$ are applied individually or combined, trends remain the same, showing the highest δ^{13}C values of planktonic foraminifera during the LGM (Fig. S5). Hence, despite the uncertainties in interpreting the absolute planktonic δ^{13}C values, the trend in $\Delta\delta^{13}$C should still provide a measure for changes in the efficiency of the BCP. Therefore, we applied a combined correction for both temperature (Bemis et al., 2000) and $[CO_3^{2-}]$ (Bijma et al., 1999), derived from foraminiferal Mg / Ca and δ^{11}B, respectively (Fig. 6c). The offset of the δ^{13}C value of the core-top sample with the modern δ^{13}C values of the DIC is approximately 2.4‰ (Kroopnick, 1985), which agrees with the applied corrections based on temperature and $[CO_3^{2-}]$ in the most recent samples (2.4‰–2.8‰; 4.9–5.4 ka).

Offsets between the δ^{13}C of the planktonic and benthic foraminifera reflect differences in the BCP but potentially also changes in the dominant water mass at the cores' locations. Intermediate depths of the South Atlantic are dominated today by the Antarctic Intermediate Water, and this likely remained the major water mass over the last glacial cycle (Pahnke et al., 2008; Howe et al., 2016; Gu et al., 2017). However, it is unclear whether the depth range of the AAIW increased (Muratli et al., 2010) or decreased (Ronge et al., 2015; Li et al., 2021) during the LGM compared to the present day. In the western Atlantic, δ^{13}C values of benthic foraminifera suggest the persistence of AAIW masses at the depth of our core site (e.g., Curry and Oppo, 2005). As our values correspond to those found in the western Atlantic (Curry and Oppo, 2005; Lacerra et al., 2019; Umling et al., 2019), a sustained influence of southern water masses is likely, with the δ^{13}C value of DIC in the AAIW during the LGM remaining relatively similar to the present day.

Variations in the stable carbon isotopic composition of surface seawater DIC are attributed to the changes in biological activity and air–sea exchange (Lynch-Stieglitz et al., 1995). While enhanced biological activity will result in an increase in δ^{13}C values of DIC, more intense air–sea exchange will contribute to a decrease. In upwelling regions, the upwelled light carbon may still result in a net decrease in δ^{13}C values despite the enhanced biological activity. The analyzed δ^{13}C values of benthic foraminifera from the LGM in this study show on average values that are 0.2‰ lower than those during the Holocene, with a minimum glacial to a maximum Holocene range of 0.4‰–1‰. This increasing trend in mid-depth benthic δ^{13}C values from glacial to interglacial agrees with the trends reported from the Brazilian Margin, where potentially both air–sea CO_2 exchange (Umling et al., 2019) and remineralization (Lacerra et al., 2019) affect the δ^{13}C

signal. Estimates of $[PO_4^{3-}]$ based on foraminiferal Ba / Ca show a general increase from glacial to interglacial, with relatively low values between 18 and 15 ka corresponding to the observed planktonic δ^{13}C minimum (Fig. S6). Although we cannot rule out a contribution of air–sea gas exchange, especially on the timescale of short-term climatic changes, we believe that the observed glacial–interglacial trend was primarily driven by a change in the BCP efficiency.

Summarizing the observed impacts, assuming a more or less stable presence of AAIW at intermediate depth and minimal impact of change in air–sea CO_2 exchange on δ^{13}C values, after correcting for offsets, a larger difference between planktonic and benthic foraminiferal δ^{13}C values during the LGM compared to the Holocene is evident (Figs. 6c and S5), suggesting a more efficient BCP.

6.3 pCO$_2$ record of the BUS over the last 27 kyr

Although δ^{11}B in foraminifera shells and δ^{13}C of alkenones are the most commonly applied methods to reconstruct pCO$_2$, these proxies are only very rarely compared in the same record. Since these proxies record different components of the speciation of carbon in seawater and have different biases, they do not necessarily have to show similar results. Here, we observe only a modest change in pH (8.08–8.23 ± 0.07, derived from foraminiferal δ^{11}B) during the last deglaciation, whereas pCO$_2$ values show a change from 180 to 280 ppm (±42 ppm, derived from δ^{13}C of alkenones; Fig. 7).

Minor variability in pH was reported previously by Raitzsch et al. (2018) for the Walvis Ridge for the same time interval, although reconstructed pH values were slightly higher (0.10–0.14 pH units). Although only minor, the offset is in line with the core studied here being closer to the upwelling area, as the major upwelling area extends only about 200 km out of the coast today (Lutjeharms and Meeuwis, 1987; Lutjeharms and Stockton, 1987). With the lowest pH values in the core of the upwelling area and values increasing towards the open ocean, the trend in the offset between the two areas is minor but in the right direction.

Using pH and total alkalinity, pCO$_2$ can be calculated, suggesting higher pCO$_2$ compared to the known atmospheric values over the past 27 kyr (Fig. 7; Petit et al., 1999). Calculated pCO$_2$ based on the foraminiferal δ^{11}B only matches seawater equilibrium values at 13.5 and 8.2 ka. While the Bølling–Allerød event marks an AMOC amplification, AMOC was reduced around 8.2 ka due to the meltwater input in the North Atlantic (Matero et al., 2017; Barber et al., 1999; Pedro et al., 2016; Blunier et al., 1997). However, the calculated pCO$_2$ values are associated with considerable uncertainty for a large part related to total alkalinity being ill-constrained. Using estimates of total alkalinity based on relative sea level change is debated (e.g., de la Vega et al., 2023), as this does not account for all changes in alkalinity on glacial–interglacial timescales. Because total alkalinity cal-
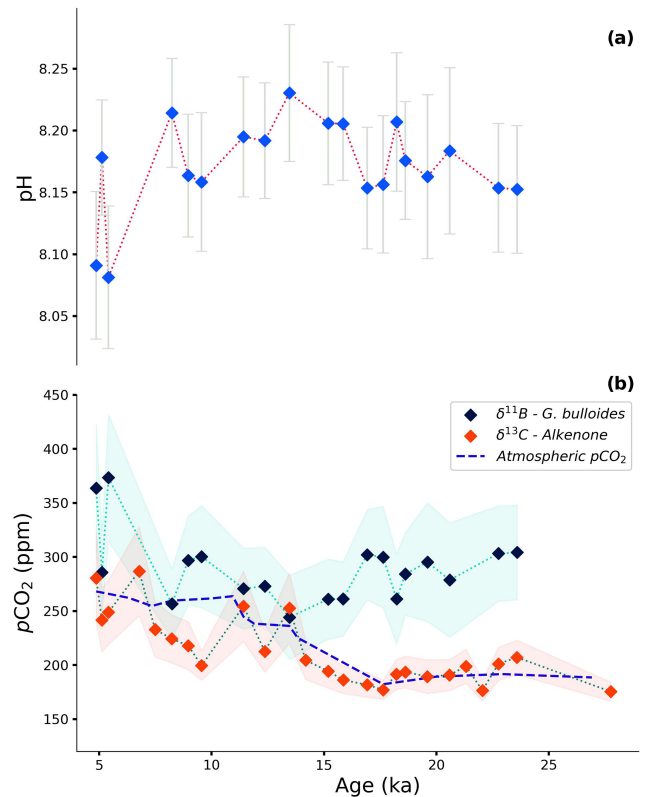
Figure 7. Reconstruction of **(a)** pH based on δ^{11}B of *G. bulloides* and **(b)** pCO$_2$ based on δ^{11}B of *G. bulloides* combined with a constant total alkalinity value of 2349 ± 11.07 µmol kg^{-1} (dark-blue diamonds) and δ^{13}C of alkenones with Ba / Ca-based $[PO_4^{3-}]$ estimates (red diamonds). The modern-day pCO$_2$ value of the AAIW is approximately 326 ppm (Lauvset et al., 2024; Salt et al., 2015). The dashed blue line shows the Vostok ice core record of pCO$_2$ (Petit et al., 1999). The shaded light-green and red areas represent the propagated error for the foraminifera- and alkenone-based reconstructions, respectively. See further details on uncertainty propagation in the text.

culated based on the relative sea level change during the last deglaciation results in only a small (less than 10 ppm) offset, we used constant alkalinity (2349 ± 11 µmol kg^{-1}; GLODAPv2023; Lauvset et al., 2024) in combination with boron-isotope-based pH to determine pCO$_2$. The trends observed here are not affected by the alkalinity values used.

The seawater pCO$_2$ reconstruction based on the δ^{13}C of alkenones follows past atmospheric pCO$_2$, known from the Vostok ice core record, well (Petit et al., 1999). This suggests that, over the interval studied here, the BUS remained more or less in equilibrium with the atmosphere with regard to CO_2 and did not act as an appreciable source or sink. An offset is observed (about 65 ppm) during the Holocene, between 11 and 7 ka, when alkenone-based reconstruction suggests somewhat lower pCO$_2$ values compared to the ice core record, although this difference falls well within the uncertainty of the proxy. This could indicate a temporary transition

of the area to a CO_2 sink as the seawater becomes undersaturated with respect to CO_2.

The good agreement between alkenone-based and ice core $p CO_2$ records suggests that previously recognized complications in applying this proxy may not be relevant in the BUS region. Adaptation of CCM by the alkenone producers can hamper the use of the proxy under low $p CO_2$ conditions (Badger, 2021). However, the mechanisms that may control CCM in the alkenone producers are not fully constrained (e.g., Reinfelder, 2011), and effectiveness of the CCM may differ between species (e.g., Goudet et al., 2020; Heureux et al., 2017). As the reconstruction of $p CO_2$ values based on alkenone $\delta^{13}C$ provided a reasonable record here and in another upwelling region (Palmer et al., 2010), application of this proxy in upwelling sites may be able to rely on the classical concept of passive diffusion of CO_2 (Bidigare et al., 1997; Laws et al., 1995). Additional uncertainty in the alkenone-based $p CO_2$ reconstruction may derive from the estimation of the b factor. Often, modern and constant $[PO_4^{3-}]$ is assumed to estimate the b factor for reconstructing $p CO_2$ (Pagani et al., 1999; Zhang et al., 2013; Pagani et al., 2005; Witkowski et al., 2020), or, assuming that the membrane permeability has not changed significantly, one can correct for the growth rate effects of the alkenone producers (Zhang et al., 2019; Zhang et al., 2020). Here, we used foraminiferal Ba / Ca, which is suggested to reflect nutrient ($[PO_4^{3-}]$) variations but does not vary with temperature, salinity, or carbon chemistry parameters (Lea and Spero, 1994; Hönisch et al., 2011), unlike other suggested nutrient proxies, such as Cd / Ca (Oppo and Rosenthal, 1994; Allen et al., 2016) and Zn / Ca (Van Dijk et al., 2017). Using the Ba / Ca approach to constrain the b factor yields 10 to 105 ppm lower $p CO_2$ values here compared to the approach of using a constant $[PO_4^{3-}]$ based on modern values over the last 27 kyr (Fig. S7). These approaches make a non-negligible difference to our conclusions, as the results based on the use of constant $[PO_4^{3-}]$ imply constant net CO_2 outgassing in the BUS over the last glacial and deglacial. However, variability in surface $p CO_2$ remains minor, causing only 32 ppm change in $p CO_2$ in the BUS over 27 kyr, which is unlikely considering the highly dynamic properties of the region on a glacial–interglacial timescale (Mollenhauer et al., 2002; McKay et al., 2016; Romero et al., 2003). Also, previous studies pointed out an overestimation of surface $p CO_2$ when constant nutrient levels are applied to constrain the b factor (Zhang et al., 2019, and references therein), which is in line with our observation when the two approaches (Ba / Ca and constant $[PO_4^{3-}]$) are compared. While the Ba / Ca method still awaits refinements in future studies, this approach may provide an efficient way to address some of the uncertainties originating from local conditions that are not targeted when constant $[PO_4^{3-}]$ values are assumed.
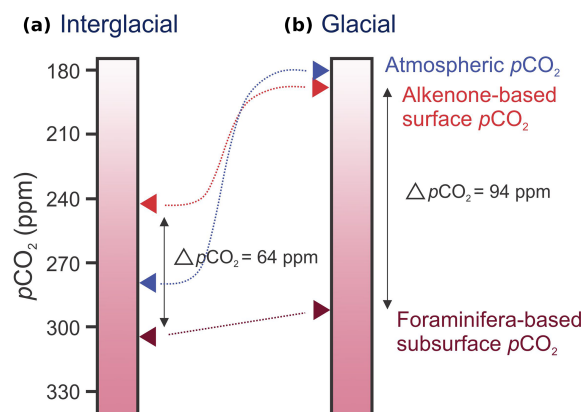
Figure 8. Schematic comparison of interglacial and glacial $p CO_2$ values. Red arrows mark average interglacial **(a)** and glacial **(b)** values calculated from the alkenone- and planktonic-foraminifera-based (pH and total alkalinity) proxies in this study.

6.4 Change in the efficiency of BCP and CO_2 disequilibrium

Most obvious from comparing the alkenone- and foraminifera-based $p CO_2$ reconstruction is the difference in amplitude of change on a glacial–interglacial timescale. While the alkenone-based reconstruction closely mimics atmospheric changes, the foraminifera-based reconstruction shows a constant $p CO_2$. This results in an interglacial difference in $p CO_2$ ($\Delta p CO_2 = p CO_{2(\text{foraminifera})} - p CO_{2(\text{alkenone})}$) of about 64 ± 20 ppm between the alkenone- and foraminifera-based reconstructions, while, during glacial times, $\Delta p CO_2$ increases to approximately 94 ± 20 ppm (Fig. 8). Because the *G. bulloides* are proliferating during the upwelling season, they likely primarily reflect the deeper upwelled water (i.e., subsurface) compared to the alkenones, which are synthesized, for example, by the surface-dwelling coccolithophorids. Note that *G. bulloides* may migrate between approximately 50 and 400 m (Rebotim et al., 2017), which can affect the calculated $p CO_2$ gradients. Still, *G. bulloides* represents a larger average depth than the alkenone-based record and hence carbon system conditions that are closer to those of the upwelled intermediate waters, i.e., the AAIW in the BUS.

Studies using foraminifera-based proxies suggested more intense upwelling during glacial times (Oberhänsli, 1991; Little et al., 1997), but, at the same time, radiolarian-based upwelling proxies indicate reduced upwelling (Des Combes and Abelmann, 2007). Due to its location and the influence of water masses both from the north and the south, cells of the BUS are characterized by different environmental conditions (e.g., temperature and nutrients; Emeis et al., 2018). During the LGM, cold source waters likely impacted the northern cells of the BUS more than its central and southern parts (Des Combes and Abelmann, 2007), affirming complexity of this upwelling system. While we may conclude that upwelling

intensities were different from one cell to another, potentially also impacted by the offshore transition of the modern strong upwelling cells (e.g., Mollenhauer et al., 2002), increased cold water input does not necessarily correlate with stronger upwelling (Des Combes and Abelmann, 2007), potentially explaining conflicting interpretations based on different proxies.

Atmospheric $p\mathrm{CO_2}$ was significantly reduced during the LGM; hence the presence of an increased amount of $\mathrm{CO_2}$ at subsurface depths implies either enhanced upwelling or that the upwelled waters were richer in $\mathrm{CO_2}$ or both. Lower atmospheric $\mathrm{CO_2}$ during the glacial is likely explained by multiple processes. The larger extent of sea ice over the glacial Southern Ocean prevented $\mathrm{CO_2}$ escaping from seawater in an area today acting as a major $\mathrm{CO_2}$ exchange region (Stephens and Keeling, 2000), whereas enhanced iron fertilization likely contributed to more efficient utilization and transport of carbon and nutrients to the deep (Martin, 1990; Martínez-García et al., 2014). Eolian transport and dissolution in the shelf regions might have provided important sources of iron at that time (Martin, 1990; Tian et al., 2023), which would locally influence air–sea carbon balance, still with minimum impact on global atmospheric $p\mathrm{CO_2}$ due to adjacent regions where excess carbon can be utilized. Also locally at the BUS, eolian transport presumably increased due to the intensified trade winds (Stuut et al., 2002), although a more humid climate may (Stuut et al., 2002; Cockcroft et al., 1987) or may not (Shi et al., 1998; Partridge et al., 1999) have prevailed in southwestern Africa during the LGM. Therefore, it remains speculative whether stronger winds may have provided sufficient iron for phytoplankton growth locally or if excess iron input in the sub-Antarctic region potentially provided a source for additional mid-depth $\mathrm{CO_2}$ storage (Martínez-García et al., 2014). Still, a more efficient biological carbon pump, as indicated by the offset between the planktonic and benthic foraminiferal carbon isotope records (Fig. 6c), suggests that an increased supply of carbon in the upwelling areas from intermediate depths to the surface may have been effectively counterbalanced.

Based on comparing $p\mathrm{CO_2}$ proxies, with *G. bulloides* primarily recording the upwelled waters and alkenones primarily recording the surface waters, we see evidence for enhanced storage of carbon at depth during the glacial. The resulting mid-depth high-$\mathrm{CO_2}$ waters also provide the source for upwelled waters in the BUS at that time, which could have resulted in the local release of (part of the) stored $\mathrm{CO_2}$ if not prevented by an efficient biological carbon pump. An increased biological pump acted as an effective cap on the stored carbon and hence contributed to preventing the release of mid-depth $\mathrm{CO_2}$ during the glacial.

7 Conclusions

Carbon system proxies were applied to demonstrate changes in inorganic carbon chemistry of the northern Benguela Upwelling System over the last 27 kyr. Temperature reconstructions based on both organic and inorganic proxies indicate that the BUS may be associated with climatic changes observed in both the Northern and Southern hemispheres. While surface values of $p\mathrm{CO_2}$ reconstructed from $\delta^{13}\mathrm{C}$ of alkenones generally track atmospheric $p\mathrm{CO_2}$, the foraminifera-based reconstruction suggests minor variation in $p\mathrm{CO_2}$ in the subsurface since the Last Glacial Maximum until the present. Hence, the increased gradient of $p\mathrm{CO_2}$ between the surface waters and depth observed for the last glacial period provides evidence for enhanced storage of carbon in the Antarctic Intermediate Water. Outgassing of $\mathrm{CO_2}$, however, could be effectively prevented by the biological carbon pump, as also indicated by the offset in the $\delta^{13}\mathrm{C}$ of planktonic and benthic foraminifera.

Author contributions. SK, LJdN, SS, and GJR designed the study. RH and ZE collected the sample material, and SK prepared and processed the samples. SK, BvdW, MTJvdM, and SM were responsible for the analysis of foraminifera and alkenones. JL and NH conducted the radiocarbon analysis. SK interpreted and visualized the data under the supervision of LJdN, SS, and GJR and drafted the paper with contribution from all co-authors.

Competing interests. The contact author has declared that none of the authors has any competing interests.

Disclaimer. Publisher's note: Copernicus Publications remains neutral with regard to jurisdictional claims made in the text, published maps, institutional affiliations, or any other geographical representation in this paper. While Copernicus Publications makes every effort to include appropriate place names, the final responsibility lies with the authors.

References

Alldredge, A. L. and Silver, M. W.: Characteristics, dynamics and significance of marine snow, Prog. Oceanogr., 20, 41–82, https://doi.org/10.1016/0079-6611(88)90053-5, 1988.

Allen, K. A., Hönisch, B., Eggins, S. M., Haynes, L. L., Rosenthal, Y., and Yu, J.: Trace element proxies for surface ocean conditions: A synthesis of culture calibrations with planktic foraminifera, Geochim. Cosmochim. Ac., 193, 197–221, https://doi.org/10.1016/j.gca.2016.08.015, 2016.

Alley, R. B.: The Younger Dryas cold interval as viewed from central Greenland, Quaternary Sci. Rev., 19, 213–226, https://doi.org/10.1016/S0277-3791(99)00062-1, 2000.

Andersen, N., Müller, P. J., Kirst, G., and Schneider, R. R.: Alkenone δ^{13}C as a Proxy for Past PCO$_2$ in Surface Waters: Results from the Late Quaternary Angola Current, in: Use of Proxies in Paleoceanography: Examples from the South Atlantic, edited by: Fischer, G. and Wefer, G., Springer Berlin Heidelberg, Berlin, Heidelberg, 469–488, https://doi.org/10.1007/978-3-642-58646-0_19, 1999.

Armstrong, R. A., Lee, C., Hedges, J. I., Honjo, S., and Wakeham, S. G.: A new, mechanistic model for organic carbon fluxes in the ocean based on the quantitative association of POC with ballast minerals, Deep-Sea Res. Pt. II, 49, 219-236, https://doi.org/10.1016/S0967-0645(01)00101-1, 2001.

Badger, M. P. S.: Alkenone isotopes show evidence of active carbon concentrating mechanisms in coccolithophores as aqueous carbon dioxide concentrations fall below 7 µmol L^{-1}, Biogeosciences, 18, 1149–1160, https://doi.org/10.5194/bg-18-1149-2021, 2021.

Bae, S. W., Lee, K. E., and Kim, K.: Use of carbon isotopic composition of alkenone as a CO$_2$ proxy in the East Sea/Japan Sea, Cont. Shelf Res., 107, 24–32, https://doi.org/10.1016/j.csr.2015.07.010, 2015.

Barber, D. C., Dyke, A., Hillaire-Marcel, C., Jennings, A. E., Andrews, J. T., Kerwin, M. W., Bilodeau, G., McNeely, R., Southon, J., Morehead, M. D., and Gagnon, J. M.: Forcing of the cold event of 8,200 years ago by catastrophic drainage of Laurentide lakes, Nature, 400, 344–348, https://doi.org/10.1038/22504, 1999.

Barker, S., Greaves, M., and Elderfield, H.: A study of cleaning procedures used for foraminiferal Mg / Ca paleothermometry, Geochem. Geophy. Geosy., 4, 8407, https://doi.org/10.1029/2003GC000559, 2003.

Bemis, B. E., Spero, H. J., Lea, D. W., and Bijma, J.: Temperature influence on the carbon isotopic composition of *Globigerina bulloides* and *Orbulina universa* (planktonic foraminifera), Mar. Micropaleontol., 38, 213–228, https://doi.org/10.1016/S0377-8398(00)00006-2, 2000.

Bice, K. L., Birgel, D., Meyers, P. A., Dahl, K. A., Hinrichs, K.-U., and Norris, R. D.: A multiple proxy and model study of Cretaceous upper ocean temperatures and atmospheric CO$_2$ concentrations, Paleoceanography, 21, PA2002, https://doi.org/10.1029/2005PA001203, 2006.

Bidigare, R. R., Fluegge, A., Freeman, K. H., Hanson, K. L., Hayes, J. M., Hollander, D., Jasper, J. P., King, L. L., Laws, E. A., and Milder, J.: Consistent fractionation of ^{13}C in nature and in the laboratory: Growth-rate effects in some haptophyte algae, Global Biogeochem. Cy., 11, 279–292, https://doi.org/10.1029/96GB03939, 1997.

Bijl, P. K., Houben, A. J. P., Schouten, S., Bohaty, S. M., Sluijs, A., Reichart, G.-J., Sinninghe Damsté, J. S., and Brinkhuis, H.: Transient Middle Eocene atmospheric CO$_2$ and temperature variations, Science, 330, 819–821, https://doi.org/10.1126/science.1193654, 2010.

Bijma, J., Spero, H., and Lea, D.: Reassessing foraminiferal stable isotope geochemistry: Impact of the oceanic carbonate system (experimental results), in: Use of proxies in paleoceanography, edited by: Fischer, G. and Wefer, G., Springer, Berlin, Heidelberg, 489–512, https://doi.org/10.1007/978-3-642-58646-0_20, 1999.

Bird, C., Darling, K. F., Russell, A. D., Davis, C. V., Fehrenbacher, J., Free, A., Wyman, M., and Ngwenya, B. T.: Cyanobacterial endobionts within a major marine planktonic calcifier (Globigerina bulloides, Foraminifera) revealed by 16S rRNA metabarcoding, Biogeosciences, 14, 901–920, https://doi.org/10.5194/bg-14-901-2017, 2017.

Blaauw, M. and Christen, J. A.: Flexible paleoclimate age-depth models using an autoregressive gamma process, Bayesian Anal., 6, 457–474, https://doi.org/10.1214/11-BA618, 2011.

Blunier, T. and Brook, E. J.: Timing of Millennial-Scale Climate Change in Antarctica and Greenland During the Last Glacial Period, Science, 291, 109–112, https://doi.org/10.1126/science.291.5501.109, 2001.

Blunier, T., Schwander, J., Stauffer, B., Stocker, T., Dällenbach, A., Indermühle, A., Tschumi, J., Chappellaz, J., Raynaud, D., and Barnola, J. M.: Timing of the Antarctic cold reversal and the atmospheric CO$_2$ increase with respect to the Younger Dryas Event, Geophys. Res. Lett., 24, 2683–2686, https://doi.org/10.1029/97GL02658, 1997.

Boer, W., Nordstad, S., Weber, M., Mertz-Kraus, R., Hönisch, B., Bijma, J., Raitzsch, M., Wilhelms-Dick, D., Foster, G. L., and Goring-Harford, H.: New calcium carbonate nano-particulate pressed powder pellet (NFHS-2-NP) for LA-ICP-OES, LA-(MC)-ICP-MS and μ XRF, Geostand. Geoanal. Res., 46, 411–432, https://doi.org/10.1111/ggr.12425, 2022.

Bolton, C. T. and Stoll, H. M.: Late Miocene threshold response of marine algae to carbon dioxide limitation, Nature, 500, 558–562, https://doi.org/10.1038/nature12448, 2013.

Bond, G., Broecker, W., Johnsen, S., McManus, J., Labeyrie, L., Jouzel, J., and Bonani, G.: Correlations between climate records from North Atlantic sediments and Greenland ice, Nature, 365, 143–147, https://doi.org/10.1038/365143a0, 1993.

Brady, R. X., Lovenduski, N. S., Alexander, M. A., Jacox, M., and Gruber, N.: On the role of climate modes in modulating the air–sea CO_2 fluxes in eastern boundary upwelling systems, Biogeosciences, 16, 329–346, https://doi.org/10.5194/bg-16-329-2019, 2019.

Broecker, W. S.: Paleocean circulation during the last deglaciation: a bipolar seesaw?, Paleoceanography, 13, 119–121, https://doi.org/10.1029/97PA03707, 1998.

Cacho, I., Grimalt, J. O., Pelejero, C., Canals, M., Sierro, F. J., Flores, J. A., and Shackleton, N.: Dansgaard-Oeschger and Heinrich event imprints in Alboran Sea paleotemperatures, Paleoceanography, 14, 698–705, https://doi.org/10.1029/1999PA900044, 1999.

Calvo, E., Pelejero, C., De Deckker, P., and Logan, G. A.: Antarctic deglacial pattern in a 30 kyr record of sea surface temperature offshore South Australia, Geophys. Res. Lett., 34, L13707, https://doi.org/10.1029/2007GL029937, 2007.

Carr, M.-E.: Estimation of potential productivity in Eastern Boundary Currents using remote sensing, Deep-Sea Res. Pt. II, 49, 59–80, https://doi.org/10.1016/S0967-0645(01)00094-7, 2001.

Chanakya, I. V. S. and Misra, S.: Accurate and precise determination of the boron isotope ratio by QQQ-ICP-MS: application to natural waters and carbonates, J. Anal. Atom. Spectrom., 37, 1327–1339, https://doi.org/10.1039/D2JA00051B, 2022.

Charles, C. D. and Morley, J. J.: The paleoceanographic significance of the radiolarian didymocyrtis tetrathalamus in Eastern Cape basin sediments, Palaeogeogr. Palaeocl., 66, 113–126, https://doi.org/10.1016/0031-0182(88)90084-3, 1988.

Chavez, F. P. and Messié, M.: A comparison of eastern boundary upwelling ecosystems, Prog. Oceanogr., 83, 80–96, https://doi.org/10.1016/j.pocean.2009.07.032, 2009.

Clark, P. U., Dyke, A. S., Shakun, J. D., Carlson, A. E., Clark, J., Wohlfarth, B., Mitrovica, J. X., Hostetler, S. W., and McCabe, A. M.: The Last Glacial Maximum, Science, 325, 710–714, https://doi.org/10.1126/science.1172873, 2009.

Cockcroft, M. J., Wilkinson, M. J., and Tyson, P. D.: The application of a present-day climatic model to the late quaternary in southern Africa, Clim. Change, 10, 161–181, https://doi.org/10.1007/BF00140253, 1987.

Conte, M., Volkman, J., and Eglinton, G.: Lipid biomarkers of the Haptophyta, in: The haptophyte algae, edited by: Green, J. C. and Leadbeater, B. S. C., Clarendon Press: Oxford, https://doi.org/10.1093/oso/9780198577720.003.0019, 1994.

Conte, M. H., Sicre, M.-A., Rühlemann, C., Weber, J. C., Schulte, S., Schulz-Bull, D., and Blanz, T.: Global temperature calibration of the alkenone unsaturation index ($U^K{}'_{37}$) in surface waters and comparison with surface sediments, Geochem. Geophy. Geosy., 7, Q02005, https://doi.org/10.1029/2005GC001054, 2006.

Curry, W. B. and Oppo, D. W.: Glacial water mass geometry and the distribution of $\delta^{13}C$ of ΣCO_2 in the western Atlantic Ocean, Paleoceanography, 20, PA1017, https://doi.org/10.1029/2004PA001021, 2005.

Damsté, J. S. S., Kuypers, M. M. M., Pancost, R. D., and Schouten, S.: The carbon isotopic response of algae, (cyano)bacteria, archaea and higher plants to the late Cenomanian perturbation of the global carbon cycle: Insights from biomarkers in black shales from the Cape Verde Basin (DSDP Site 367), Org. Geochem., 39, 1703–1718, https://doi.org/10.1016/j.orggeochem.2008.01.012, 2008.

Davis, C. V., Fehrenbacher, J. S., Benitez-Nelson, C., and Thunell, R. C.: Trace element heterogeneity across individual planktic foraminifera from the modern Cariaco Basin, J. Foramin. Res., 50, 204–218, https://doi.org/10.2113/gsjfr.50.2.204, 2020.

De La Rocha, C. L. and Passow, U.: Factors influencing the sinking of POC and the efficiency of the biological carbon pump, Deep-Sea Res. Pt. II, 54, 639–658, https://doi.org/10.1016/j.dsr2.2007.01.004, 2007.

de la Vega, E., Chalk, T. B., Hain, M. P., Wilding, M. R., Casey, D., Gledhill, R., Luo, C., Wilson, P. A., and Foster, G. L.: Orbital CO_2 reconstruction using boron isotopes during the late Pleistocene, an assessment of accuracy, Clim. Past, 19, 2493–2510, https://doi.org/10.5194/cp-19-2493-2023, 2023.

de Nooijer, L. J., Spero, H., Erez, J., Bijma, J., and Reichart, G.-J.: Biomineralization in perforate foraminifera, Earth-Sci. Rev., 135, 48–58, https://doi.org/10.1016/j.earscirev.2014.03.013, 2014.

de Villiers, S., Greaves, M., and Elderfield, H.: An intensity ratio calibration method for the accurate determination of Mg / Ca and Sr/Ca of marine carbonates by ICP-AES, Geochem. Geophy. Geosy., 3, 1001, https://doi.org/10.1029/2001GC000169, 2002.

Degens, E. T., Guillard, R. R. L., Sackett, W. M., and Hellebust, J. A.: Metabolic fractionation of carbon isotopes in marine plankton—I. Temperature and respiration experiments, Deep-Sea Res., 15, 1–9, https://doi.org/10.1016/0011-7471(68)90024-7, 1968.

Dekens, P. S., Lea, D. W., Pak, D. K., and Spero, H. J.: Core top calibration of Mg / Ca in tropical foraminifera: Refining paleotemperature estimation, Geochem. Geophy. Geosy., 3, 1–29, https://doi.org/10.1029/2001GC000200, 2002.

Denton, G. H., Anderson, R. F., Toggweiler, J. R., Edwards, R. L., Schaefer, J. M., and Putnam, A. E.: The Last Glacial Termination, Science, 328, 1652–1656, https://doi.org/10.1126/science.1184119, 2010.

Des Combes, H. J. and Abelmann, A.: A 350-ky radiolarian record off Lüderitz, Namibia–evidence for changes in the upwelling regime, Mar. Micropaleontol., 62, 194–210, https://doi.org/10.1016/j.marmicro.2006.08.004, 2007.

DeVries, T. and Weber, T.: The export and fate of organic matter in the ocean: New constraints from combining satellite and oceanographic tracer observations, Global Biogeochem. Cy., 31, 535–555, https://doi.org/10.1002/2016GB005551, 2017.

Dewar, G., Reimer, P. J., Sealy, J., and Woodborne, S.: Late-Holocene marine radiocarbon reservoir correction (ΔR) for the west coast of South Africa, Holocene, 22, 1481–1489, https://doi.org/10.1177/0959683612449755, 2012.

Dickson, A. G.: Thermodynamics of the dissociation of boric acid in synthetic seawater from 273.15 to 318.15 K, Deep-Sea Res. Pt. I, 37, 755–766, https://doi.org/10.1016/0198-0149(90)90004-F, 1990.

Diester-Haass, L., Meyers, P. A., and Rothe, P.: The Benguela Current and associated upwelling on the southwest African

Margin: a synthesis of the Neogene-Quaternary sedimentary record at DSDP sites 362 and 532, Geological Society, London, Special Publications, 64, 331–342, https://doi.org/10.1144/GSL.SP.1992.064.01.22, 1992.

Ducklow, H. W., Steinberg, D. K., and Buesseler, K. O.: Upper ocean carbon export and the biological pump, Oceanography, 14, 50–58, 2001.

Dueñas-Bohórquez, A., da Rocha, R. E., Kuroyanagi, A., Bijma, J., and Reichart, G.-J.: Effect of salinity and seawater calcite saturation state on Mg and Sr incorporation in cultured planktonic foraminifera, Mar. Micropaleontol., 73, 178–189, https://doi.org/10.1016/j.marmicro.2009.09.002, 2009.

Emeis, K., Eggert, A., Flohr, A., Lahajnar, N., Nausch, G., Neumann, A., Rixen, T., Schmidt, M., Van der Plas, A., and Wasmund, N.: Biogeochemical processes and turnover rates in the Northern Benguela Upwelling System, J. Mar. Syst., 188, 63–80, https://doi.org/10.1016/j.jmarsys.2017.10.001, 2018.

Erez, J.: The source of ions for biomineralization in foraminifera and their implications for paleoceanographic proxies, Rev. Mineral. Geochem., 54, 115–149, https://doi.org/10.2113/0540115, 2003.

Fahrni, S. M., Wacker, L., Synal, H. A., and Szidat, S.: Improving a gas ion source for ^{14}C AMS, Nucl. Instrum. Meth. B, 294, 320–327, https://doi.org/10.1016/j.nimb.2012.03.037, 2013.

Flores, J.-A., Gersonde, R., and Sierro, F. J.: Pleistocene fluctuations in the Agulhas Current Retroflection based on the calcareous plankton record, Mar. Micropaleontol., 37, 1–22, https://doi.org/10.1016/S0377-8398(99)00012-2, 1999.

Foster, G. L. and Rae, J. W.: Reconstructing ocean pH with boron isotopes in foraminifera, Annu. Rev. Earth Planet. Sci., 44, 207–237, https://doi.org/10.1146/annurev-earth-060115-012226, 2016.

Foster, G. L., Pogge von Strandmann, P. A. E., and Rae, J. W. B.: Boron and magnesium isotopic composition of seawater, Geochem. Geophy. Geosy., 11, Q08015, https://doi.org/10.1029/2010GC003201, 2010.

Fowler, S. W. and Knauer, G. A.: Role of large particles in the transport of elements and organic compounds through the oceanic water column, Prog. Oceanogr., 16, 147–194, https://doi.org/10.1016/0079-6611(86)90032-7, 1986.

Francois, R., Honjo, S., Krishfield, R., and Manganini, S.: Factors controlling the flux of organic carbon to the bathypelagic zone of the ocean, Global Biogeochem. Cy., 16, 34-31–34-20, https://doi.org/10.1029/2001GB001722, 2002.

Franzese, A. M., Hemming, S. R., Goldstein, S. L., and Anderson, R. F.: Reduced Agulhas Leakage during the Last Glacial Maximum inferred from an integrated provenance and flux study, Earth. Planet. Sc. Lett., 250, 72–88, https://doi.org/10.1016/j.epsl.2006.07.002, 2006.

Gaillardet, J., Lemarchand, D., Göpel, C., and Manhès, G.: Evaporation and sublimation of boric acid: Application for boron purification from organic rich solutions, Geostandard. Newslett., 25, 67–75, https://doi.org/10.1111/j.1751-908X.2001.tb00788.x, 2001.

Gordon, A. L.: Interocean exchange of thermocline water, J. Geophys. Res.-Oceans, 91, 5037–5046, https://doi.org/10.1029/JC091iC04p05037, 1986.

Goudet, M. M., Orr, D. J., Melkonian, M., Müller, K. H., Meyer, M. T., Carmo-Silva, E., and Griffiths, H.: Rubisco and carbon-concentrating mechanism co-evolution across chlorophyte and streptophyte green algae, New Phytol., 227, 810–823, https://doi.org/10.1111/nph.16577, 2020.

Gray, W. R. and Evans, D.: Nonthermal influences on Mg / Ca in planktonic foraminifera: A review of culture studies and application to the last glacial maximum, Paleoceanogr. Paleoclimatol., 34, 306–315, https://doi.org/10.1029/2018PA003517, 2019.

Gray, W. R., Weldeab, S., Lea, D. W., Rosenthal, Y., Gruber, N., Donner, B., and Fischer, G.: The effects of temperature, salinity, and the carbonate system on Mg / Ca in *Globigerinoides ruber* (white): A global sediment trap calibration, Earth. Planet. Sc. Lett., 482, 607–620, https://doi.org/10.1016/j.epsl.2017.11.026, 2018.

Gregor, L. and Monteiro, P. M.: Is the southern Benguela a significant regional sink of CO_2?, S. Afr. J. Sci., 109, 1–5, https://doi.org/10.1590/sajs.2013/20120094, 2013.

Gruber, N., Gloor, M., Mikaloff Fletcher, S. E., Doney, S. C., Dutkiewicz, S., Follows, M. J., Gerber, M., Jacobson, A. R., Joos, F., and Lindsay, K.: Oceanic sources, sinks, and transport of atmospheric CO_2, Global Biogeochem. Cy., 23, GB1005, https://doi.org/10.1029/2008GB003349, 2009.

Gu, S., Liu, Z., Zhang, J., Rempfer, J., Joos, F., and Oppo, D. W.: Coherent response of Antarctic Intermediate Water and Atlantic Meridional Overturning Circulation during the last deglaciation: Reconciling contrasting neodymium isotope reconstructions from the tropical Atlantic, Paleoceanography, 32, 1036–1053, https://doi.org/10.1002/2017PA003092, 2017.

Hain, M. P., Sigman, D., and Haug, G.: The biological pump in the past, Reference Module in Earth Systems and Environmental Sciences, Treatise on Geochemistry (Second Edition), Oceans and Marine Geochemistry, 8, 485–517, https://doi.org/10.1016/B978-0-08-095975-7.00618-5, 2014.

Hales, B., Takahashi, T., and Bandstra, L.: Atmospheric CO_2 uptake by a coastal upwelling system, Global Biogeochem. Cy., 19, GB1009, https://doi.org/10.1029/2004GB002295, 2005.

Hart, T. J. and Currie, R. I.: The benguela current, Discov. Rep., 31, 123–297, 1960.

Hayes, J. M.: Factors controlling ^{13}C contents of sedimentary organic compounds: Principles and evidence, Mar. Geol., 113, 111–125, https://doi.org/10.1016/0025-3227(93)90153-M, 1993.

Heaton, T. J., Köhler, P., Butzin, M., Bard, E., Reimer, R. W., Austin, W. E. N., Bronk Ramsey, C., Grootes, P. M., Hughen, K. A., Kromer, B., Reimer, P. J., Adkins, J., Burke, A., Cook, M. S., Olsen, J., and Skinner, L. C.: Marine20 – The Marine Radiocarbon Age Calibration Curve (0–55,000 cal BP), Radiocarbon, 62, 779–820, https://doi.org/10.1017/RDC.2020.68, 2020.

Hemleben, C., Spindler, M., and Anderson, O. R.: Modern planktonic foraminifera, Springer-Verlag, New York, https://doi.org/10.1007/978-1-4612-3544-6, 1989.

Hemming, N. and Hanson, G.: Boron isotopic composition and concentration in modern marine carbonates, Geochim. Cosmochim. Ac., 56, 537–543, https://doi.org/10.1016/0016-7037(92)90151-8, 1992.

Henehan, M. J., Rae, J. W. B., Foster, G. L., Erez, J., Prentice, K. C., Kucera, M., Bostock, H. C., Martínez-Botí, M. A., Milton, J. A., Wilson, P. A., Marshall, B. J., and Elliott, T.: Calibration of the boron isotope proxy in the planktonic foraminifera *Globigerinoides ruber* for use in palaeo-

CO$_2$ reconstruction, Earth. Planet. Sc. Lett., 364, 111–122, https://doi.org/10.1016/j.epsl.2012.12.029, 2013.

Henehan, M. J., Foster, G. L., Bostock, H. C., Greenop, R., Marshall, B. J., and Wilson, P. A.: A new boron isotope-pH calibration for *Orbulina universa* , with implications for understanding and accounting for "vital effects", Earth. Planet. Sc. Lett., 454, 282–292, https://doi.org/10.1016/j.epsl.2016.09.024, 2016.

Henson, S. A., Sanders, R., Madsen, E., Morris, P. J., Le Moigne, F., and Quartly, G. D.: A reduced estimate of the strength of the ocean's biological carbon pump, Geophys. Res. Lett., 38, L04606, https://doi.org/10.1029/2011GL046735, 2011.

Heureux, A. M. C., Young, J. N., Whitney, S. M., Eason-Hubbard, M. R., Lee, R. B. Y., Sharwood, R. E., and Rickaby, R. E. M.: The role of Rubisco kinetics and pyrenoid morphology in shaping the CCM of haptophyte microalgae, J. Exp. Bot., 68, 3959–3969, https://doi.org/10.1093/jxb/erx179, 2017.

Hill, A. E.: Eastern Ocean Boundaries, Sea, VII, 29–67, 1998.

Hilting, A. K., Kump, L. R., and Bralower, T. J.: Variations in the oceanic vertical carbon isotope gradient and their implications for the Paleocene-Eocene biological pump, Paleoceanography, 23, PA3222, https://doi.org/10.1029/2007PA001458, 2008.

Hodell, D. A., Nicholl, J. A., Bontognali, T. R. R., Danino, S., Dorador, J., Dowdeswell, J. A., Einsle, J., Kuhlmann, H., Martrat, B., Mleneck-Vautravers, M. J., Rodríguez-Tovar, F. J., and Röhl, U.: Anatomy of Heinrich Layer 1 and its role in the last deglaciation, Paleoceanography, 32, 284–303, https://doi.org/10.1002/2016PA003028, 2017.

Hönisch, B. and Hemming, N. G.: Ground-truthing the boron isotope-paleo-pH proxy in planktonic foraminifera shells: Partial dissolution and shell size effects, Paleoceanography, 19, PA4010, https://doi.org/10.1029/2004PA001026, 2004.

Hönisch, B., Allen, K. A., Russell, A. D., Eggins, S. M., Bijma, J., Spero, H. J., Lea, D. W., and Yu, J.: Planktic foraminifers as recorders of seawater Ba/Ca, Mar. Micropaleontol., 79, 52–57, https://doi.org/10.1016/j.marmicro.2011.01.003, 2011.

Hover, V. C., Walter, L. M., and Peacor, D. R.: Early marine diagenesis of biogenic aragonite and Mg-calcite: new constraints from high-resolution STEM and AEM analyses of modern platform carbonates, Chem. Geol., 175, 221–248, https://doi.org/10.1016/S0009-2541(00)00326-0, 2001.

Howe, J. N. W., Piotrowski, A. M., Oppo, D. W., Huang, K.-F., Mulitza, S., Chiessi, C. M., and Blusztajn, J.: Antarctic intermediate water circulation in the South Atlantic over the past 25,000 years, Paleoceanography, 31, 1302–1314, https://doi.org/10.1002/2016PA002975, 2016.

Hughes, P. D., Gibbard, P. L., and Ehlers, J.: Timing of glaciation during the last glacial cycle: evaluating the concept of a global "Last Glacial Maximum" (LGM), Earth-Sci. Rev., 125, 171–198, https://doi.org/10.1016/j.earscirev.2013.07.003, 2013.

Humphreys, M. P., Lewis, E. R., Sharp, J. D., and Pierrot, D.: PyCO2SYS v1.8: marine carbonate system calculations in Python, Geosci. Model Dev., 15, 15–43, https://doi.org/10.5194/gmd-15-15-2022, 2022.

Jasper, J. P. and Hayes, J. M.: A carbon isotope record of CO$_2$ levels during the late Quaternary, Nature, 347, 462–464, https://doi.org/10.1038/347462a0, 1990.

Jasper, J. P., Hayes, J., Mix, A. C., and Prahl, F. G.: Photosynthetic fractionation of ^{13}C and concentrations of dissolved CO$_2$ in the central equatorial Pacific during the last 255,000 years, Pale-

oceanography, 9, 781–798, https://doi.org/10.1029/94PA02116, 1994.

Jonkers, L., van Heuven, S., Zahn, R., and Peeters, F. J. C.: Seasonal patterns of shell flux, δ^{18}O and δ^{13}C of small and large *N.pachyderma* (s) and *G.bulloides* in the subpolar North Atlantic, Paleoceanography, 28, 164–174, https://doi.org/10.1002/palo.20018, 2013.

Jouzel, J., Masson-Delmotte, V., Cattani, O., Dreyfus, G., Falourd, S., Hoffmann, G., Minster, B., Nouet, J., Barnola, J. M., Chappellaz, J., Fischer, H., Gallet, J. C., Johnsen, S., Leuenberger, M., Loulergue, L., Luethi, D., Oerter, H., Parrenin, F., Raisbeck, G., Raynaud, D., Schilt, A., Schwander, J., Selmo, E., Souchez, R., Spahni, R., Stauffer, B., Steffensen, J. P., Stenni, B., Stocker, T. F., Tison, J. L., Werner, M., and Wolff, E. W.: Orbital and Millennial Antarctic Climate Variability over the Past 800,000 Years, Science, 317, 793–796, https://doi.org/10.1126/science.1141038, 2007.

Kahn, M.: Non-equilibrium oxygen and carbon isotopic fractionation in tests of living planktonic-foraminifera, Oceanol. Acta, 2, 195–208, 1979.

Kahn, M. I. and Williams, D. F.: Oxygen and carbon isotopic composition of living planktonic foraminifera from the northeast Pacific Ocean, Palaeogeogr. Palaeocl., 33, 47–69, https://doi.org/10.1016/0031-0182(81)90032-8, 1981.

Kämpf, J. and Chapman, P.: Upwelling systems of the world, Springer Cham, https://doi.org/10.1007/978-3-319-42524-5, 2016.

Kaplan, M. R., Schaefer, J. M., Denton, G. H., Barrell, D. J. A., Chinn, T. J. H., Putnam, A. E., Andersen, B. G., Finkel, R. C., Schwartz, R., and Doughty, A. M.: Glacier retreat in New Zealand during the Younger Dryas stadial, Nature, 467, 194–197, https://doi.org/10.1038/nature09313, 2010.

Karancz, S., de Nooijer, L. J., van der Wagt, B., van der Meer, M. T. J., Misra, S., Hennekam, R., Erdem, Z., Lattaud, J., Haghipour, N., Schouten, S., and Reichart, G.-J.: Dataset belonging to "Contrasts in the marine inorganic carbon chemistry of the Benguela Upwelling System since the Last Glacial Maximum" (V5), NIOZ [data set], https://doi.org/10.25850/nioz/7b.b.lh, 2024.

Key, R. M., Olsen, A., van Heuven, S., Lauvset, S. K., Velo, A., Lin, X., Schirnick, C., Kozyr, A., Tanhua, T., Hoppema, M., Jutterström, S., Steinfeldt, R., Jeansson, E., Ishii, M., Perez, F. F., and Suzuki, T.: Global Ocean Data Analysis Project, Version 2 (GLODAPv2), ORNL/CDIAC-162, NDP-093, Carbon Dioxide Inf. Anal. Cent. Oak Ridge Natl. Lab. Oak Ridge, TN, https://doi.org/10.3334/CDIAC/OTG.NDP093_GLODAPv2, 2015.

Kirst, G. J., Schneider, R. R., Müller, P. J., von Storch, I., and Wefer, G.: Late Quaternary temperature variability in the Benguela Current System derived from alkenones, Quaternary Res., 52, 92–103, https://doi.org/10.1006/qres.1999.2040, 1999.

Klaas, C. and Archer, D. E.: Association of sinking organic matter with various types of mineral ballast in the deep sea: Implications for the rain ratio, Global Biogeochem. Cy., 16, 63-61–63-14, https://doi.org/10.1029/2001GB001765, 2002.

Klochko, K., Kaufman, A. J., Yao, W., Byrne, R. H., and Tossell, J. A.: Experimental measurement of boron isotope fractionation in seawater, Earth Planet. Sc. Lett., 248, 276–285, https://doi.org/10.1016/j.epsl.2006.05.034, 2006.

Knorr, G. and Lohmann, G.: Southern Ocean origin for the resumption of Atlantic thermohaline circulation during deglaciation, Nature, 424, 532–536, https://doi.org/10.1038/nature01855, 2003.

Kohfeld, K. E., Quéré, C. L., Harrison, S. P., and Anderson, R. F.: Role of marine biology in glacial-interglacial CO_2 cycles, Science, 308, 74–78, https://doi.org/10.1126/science.1105375, 2005.

Kozdon, R., Kelly, D. C., Kitajima, K., Strickland, A., Fournelle, J. H., and Valley, J. W.: In situ $\delta^{18}O$ and Mg / Ca analyses of diagenetic and planktic foraminiferal calcite preserved in a deep-sea record of the Paleocene-Eocene thermal maximum, Paleoceanography, 28, 517–528, https://doi.org/10.1002/palo.20048, 2013.

Kroopnick, P.: The distribution of ^{13}C in the Atlantic Ocean, Earth. Planet. Sc. Lett., 49, 469–484, https://doi.org/10.1016/0012-821X(80)90088-6, 1980.

Kroopnick, P. M.: The distribution of ^{13}C of ΣCO_2 in the world oceans, Deep-Sea Res. Pt. I., 32, 57-84, https://doi.org/10.1016/0198-0149(85)90017-2, 1985.

Kwon, E. Y., Primeau, F., and Sarmiento, J. L.: The impact of remineralization depth on the air–sea carbon balance, Nat. Geosci., 2, 630–635, https://doi.org/10.1038/ngeo612, 2009.

Lacerra, M., Lund, D. C., Gebbie, G., Oppo, D. W., Yu, J., Schmittner, A., and Umling, N. E.: Less remineralized carbon in the intermediate-depth South Atlantic during Heinrich Stadial 1, Paleoceanogr. Paleoclimatol., 34, 1218–1233, https://doi.org/10.1029/2018PA003537, 2019.

Lamy, F., Kaiser, J., Arz, H. W., Hebbeln, D., Ninnemann, U., Timm, O., Timmermann, A., and Toggweiler, J. R.: Modulation of the bipolar seesaw in the Southeast Pacific during Termination 1, Earth. Planet. Sc. Lett., 259, 400–413, https://doi.org/10.1016/j.epsl.2007.04.040, 2007.

Laruelle, G. G., Lauerwald, R., Pfeil, B., and Regnier, P.: Regionalized global budget of the CO_2 exchange at the air-water interface in continental shelf seas, Global Biogeochem. Cy., 28, 1199–1214, https://doi.org/10.1002/2014GB004832, 2014.

Lauvset, S. K., Lange, N., Tanhua, T., Bittig, H. C., Olsen, A., Kozyr, A., Álvarez, M., Azetsu-Scott, K., Brown, P. J., Carter, B. R., Cotrim da Cunha, L., Hoppema, M., Humphreys, M. P., Ishii, M., Jeansson, E., Murata, A., Müller, J. D., Pérez, F. F., Schirnick, C., Steinfeldt, R., Suzuki, T., Ulfsbo, A., Velo, A., Woosley, R. J., and Key, R. M.: The annual update GLODAPv2.2023: the global interior ocean biogeochemical data product, Earth Syst. Sci. Data, 16, 2047–2072, https://doi.org/10.5194/essd-16-2047-2024, 2024.

Laws, E. A., Popp, B. N., Bidigare, R. R., Kennicutt, M. C., and Macko, S. A.: Dependence of phytoplankton carbon isotopic composition on growth rate and $[CO_2]_{aq}$: Theoretical considerations and experimental results, Geochim. Cosmochim. Ac., 59, 1131–1138, https://doi.org/10.1016/0016-7037(95)00030-4, 1995.

Laws, E. A., Falkowski, P. G., Smith Jr., W. O., Ducklow, H., and McCarthy, J. J.: Temperature effects on export production in the open ocean, Global Biogeochem. Cy., 14, 1231–1246, https://doi.org/10.1029/1999GB001229, 2000.

Lea, D. and Boyle, E.: Barium content of benthic foraminifera controlled by bottom-water composition, Nature, 338, 751–753, https://doi.org/10.1038/338751a0, 1989.

Lea, D. W. and Boyle, E. A.: A 210,000-year record of barium variability in the deep northwest Atlantic Ocean, Nature, 347, 269–272, https://doi.org/10.1038/347269a0, 1990a.

Lea, D. W. and Boyle, E. A.: Foraminiferal reconstruction of barium distributions in water masses of the glacial oceans, Paleoceanography, 5, 719–742, https://doi.org/10.1029/PA005i005p00719, 1990b.

Lea, D. W. and Boyle, E. A.: Barium in planktonic foraminifera, Geochim. Cosmochim. Ac., 55, 3321–3331, https://doi.org/10.1016/0016-7037(91)90491-M, 1991.

Lea, D. W. and Spero, H. J.: Assessing the reliability of paleochemical tracers: Barium uptake in the shells of planktonic foraminifera, Paleoceanography, 9, 445–452, https://doi.org/10.1029/94PA00151, 1994.

Leduc, G., Schneider, R., Kim, J. H., and Lohmann, G.: Holocene and Eemian sea surface temperature trends as revealed by alkenone and Mg / Ca paleothermometry, Quaternary Sci. Rev., 29, 989–1004, https://doi.org/10.1016/j.quascirev.2010.01.004, 2010.

Lessa, D., Morard, R., Jonkers, L., Venancio, I. M., Reuter, R., Baumeister, A., Albuquerque, A. L., and Kucera, M.: Distribution of planktonic foraminifera in the subtropical South Atlantic: depth hierarchy of controlling factors, Biogeosciences, 17, 4313–4342, https://doi.org/10.5194/bg-17-4313-2020, 2020.

Li, L., Liu, Z., Zhu, C., He, C., and Otto-Bliesner, B.: Shallowing Glacial Antarctic Intermediate Water by changes in sea ice and hydrological cycle, Geophys. Res. Lett., 48, e2021GL094317, https://doi.org/10.1029/2021GL094317, 2021.

Little, M., Schneider, R., Kroon, D., Price, B., Bickert, T., and Wefer, G.: Rapid palaeoceanographic changes in the Benguela Upwelling System for the last 160,000 years as indicated by abundances of planktonic foraminifera, Palaeogeogr. Palaeocl., 130, 135–161, https://doi.org/10.1016/S0031-0182(96)00136-8, 1997.

Lloyd, N. S., Sadekov, A. Y., and Misra, S.: Application of 10^{13} ohm Faraday cup current amplifiers for boron isotopic analyses by solution mode and laser ablation multicollector inductively coupled plasma mass spectrometry, Rapid Commun. Mass Spectrom., 32, 9–18, https://doi.org/10.1002/rcm.8009, 2018.

Longhurst, A. R. and Glen Harrison, W.: The biological pump: Profiles of plankton production and consumption in the upper ocean, Prog. Oceanogr., 22, 47–123, https://doi.org/10.1016/0079-6611(89)90010-4, 1989.

Lutjeharms, J. and Meeuwis, J.: The extent and variability of South-East Atlantic upwelling, S. Afr. J. Marine Sci., 5, 51–62, https://doi.org/10.2989/025776187784522621, 1987.

Lutjeharms, J. and Valentine, H.: Water types and volumetric considerations of the South-East Atlantic upwelling regime, S. Afr. J. Marine Sci., 5, 63–71, https://doi.org/10.2989/025776187784522487, 1987.

Lutjeharms, J. R. E. and Stockton, P. L.: Kinematics of the upwelling front off southern Africa, S. Afr. J. Marine Sci., 5, 35–49, https://doi.org/10.2989/025776187784522612, 1987.

Lynch-Stieglitz, J., Stocker, T. F., Broecker, W. S., and Fairbanks, R. G.: The influence of air-sea exchange on the isotopic composition of oceanic carbon: Observations and modeling, Global Biogeochem. Cy., 9, 653–665, https://doi.org/10.1029/95GB02574, 1995.

Martin, J. H.: Glacial-interglacial CO_2 change: The iron hypothesis, Paleoceanography, 5, 1–13, https://doi.org/10.1029/PA005i001p00001, 1990.

Martin, P. A. and Lea, D. W.: Comparison of water mass changes in the deep tropical Atlantic derived from Cd/Ca and carbon isotope records: Implications for changing Ba composition of Deep Atlantic Water Masses, Paleoceanography, 13, 572–585, https://doi.org/10.1029/98PA02670, 1998.

Martinez-Boti, M. A., Marino, G., Foster, G. L., Ziveri, P., Henehan, M. J., Rae, J. W., Mortyn, P. G., and Vance, D.: Boron isotope evidence for oceanic carbon dioxide leakage during the last deglaciation, Nature, 518, 219–222, https://doi.org/10.1038/nature14155, 2015.

Martínez-García, A., Sigman, D. M., Ren, H., Anderson, R. F., Straub, M., Hodell, D. A., Jaccard, S. L., Eglinton, T. I., and Haug, G. H.: Iron fertilization of the Subantarctic Ocean during the Last Ice Age, Science, 343, 1347–1350, https://doi.org/10.1126/science.1246848, 2014.

Mashiotta, T. A., Lea, D. W., and Spero, H. J.: Glacial–interglacial changes in Subantarctic sea surface temperature and δ^{18}O-water using foraminiferal Mg, Earth Planet. Sc. Lett., 170, 417–432, https://doi.org/10.1016/S0012-821X(99)00116-8, 1999.

Matero, I. S. O., Gregoire, L. J., Ivanovic, R. F., Tindall, J. C., and Haywood, A. M.: The 8.2 ka cooling event caused by Laurentide ice saddle collapse, Earth Planet. Sc. Lett., 473, 205–214, https://doi.org/10.1016/j.epsl.2017.06.011, 2017.

McKay, C. L., Filipsson, H. L., Romero, O. E., Stuut, J. B. W., and Björck, S.: The interplay between the surface and bottom water environment within the Benguela Upwelling System over the last 70 ka, Paleoceanography, 31, 266–285, https://doi.org/10.1002/2015PA002792, 2016.

McManus, J. F., Bond, G. C., Broecker, W. S., Johnsen, S., Labeyrie, L., and Higgins, S.: High-resolution climate records from the North Atlantic during the last interglacial, Nature, 371, 326–329, https://doi.org/10.1038/371326a0, 1994.

McManus, J. F., Francois, R., Gherardi, J. M., Keigwin, L. D., and Brown-Leger, S.: Collapse and rapid resumption of Atlantic meridional circulation linked to deglacial climate changes, Nature, 428, 834–837, https://doi.org/10.1038/nature02494, 2004.

Mekik, F., François, R., and Soon, M.: A novel approach to dissolution correction of Mg / Ca–based paleothermometry in the tropical Pacific, Paleoceanography, 22, PA3217, https://doi.org/10.1029/2007PA001504, 2007.

Metcalfe, B., Feldmeijer, W., de Vringer-Picon, M., Brummer, G.-J. A., Peeters, F. J. C., and Ganssen, G. M.: Late Pleistocene glacial–interglacial shell-size–isotope variability in planktonic foraminifera as a function of local hydrography, Biogeosciences, 12, 4781–4807, https://doi.org/10.5194/bg-12-4781-2015, 2015.

Mezger, E., De Nooijer, L., Boer, W., Brummer, G., and Reichart, G.: Salinity controls on Na incorporation in Red Sea planktonic foraminifera, Paleoceanography, 31, 1562–1582, https://doi.org/10.1002/2016PA003052, 2016.

Misra, S., Owen, R., Kerr, J., Greaves, M., and Elderfield, H.: Determination of δ^{11}B by HR-ICP-MS from mass limited samples: Application to natural carbonates and water samples, Geochim. Cosmochim. Ac., 140, 531–552, https://doi.org/10.1016/j.gca.2014.05.047, 2014.

Mollenhauer, G., Schneider, R. R., Müller, P. J., Spieß, V., and Wefer, G.: Glacial/interglacial variablity in the Benguela up-

welling system: Spatial distribution and budgets of organic carbon accumulation, Global Biogeochem. Cy., 16, 81-81–81-15, https://doi.org/10.1029/2001GB001488, 2002.

Mollenhauer, G., Eglinton, T. I., Ohkouchi, N., Schneider, R. R., Müller, P. J., Grootes, P. M., and Rullkötter, J.: Asynchronous alkenone and foraminifera records from the Benguela Upwelling System, Geochim. Cosmochim. Ac., 67, 2157–2171, https://doi.org/10.1016/s0016-7037(03)00168-6, 2003.

Mook, W. G., Bommerson, J. C., and Staverman, W. H.: Carbon isotope fractionation between dissolved bicarbonate and gaseous carbon dioxide, Earth Planet. Sc. Lett., 22, 169–176, https://doi.org/10.1016/0012-821X(74)90078-8, 1974.

Muller-Karger, F. E., Varela, R., Thunell, R., Luerssen, R., Hu, C., and Walsh, J. J.: The importance of continental margins in the global carbon cycle, Geophys. Res. Lett., 32, L01602, https://doi.org/10.1029/2004GL021346, 2005.

Muratli, J. M., Chase, Z., Mix, A. C., and McManus, J.: Increased glacial-age ventilation of the Chilean margin by Antarctic Intermediate Water, Nat. Geosci., 3, 23–26, https://doi.org/10.1038/ngeo715, 2010.

Ni, S., Quintana Krupinski, N. B., Groeneveld, J., Persson, P., Somogyi, A., Brinkmann, I., Knudsen, K. L., Seidenkrantz, M. S., and Filipsson, H. L.: Early diagenesis of foraminiferal calcite under anoxic conditions: A case study from the Landsort Deep, Baltic Sea (IODP Site M0063), Chem. Geol., 558, 119871, https://doi.org/10.1016/j.chemgeo.2020.119871, 2020.

North Greenland Ice Core Project members: High-resolution record of Northern Hemisphere climate extending into the last interglacial period, Nature, 431, 147–151, https://doi.org/10.1038/nature02805, 2004.

Oberhänsli, H.: Upwelling signals at the northeastern Walvis Ridge during the past 500,000 years, Paleoceanography, 6, 53–71, https://doi.org/10.1029/90PA02106, 1991.

Okai, T., Suzuki, A., Terashima, S., Inoue, M., Nohara, M., Kawahata, H., and Imai, N.: Collaborative analysis of GSJ/AIST geochemical reference materials JCp-1 (Coral) and JCt-1 (Giant Clam), Geochem, 38, 281–286, 2004.

Olsen, A., Key, R. M., van Heuven, S., Lauvset, S. K., Velo, A., Lin, X., Schirnick, C., Kozyr, A., Tanhua, T., Hoppema, M., Jutterström, S., Steinfeldt, R., Jeansson, E., Ishii, M., Pérez, F. F., and Suzuki, T.: The Global Ocean Data Analysis Project version 2 (GLODAPv2) – an internally consistent data product for the world ocean, Earth Syst. Sci. Data, 8, 297–323, https://doi.org/10.5194/essd-8-297-2016, 2016.

Oppo, D. W. and Fairbanks, R. G.: Carbon isotope composition of tropical surface water during the past 22,000 years, Paleoceanography, 4, 333–351, https://doi.org/10.1029/PA004i004p00333, 1989.

Oppo, D. W. and Rosenthal, Y.: Cd/Ca changes in a Deep Cape Basin Core over the past 730,000 years: Response of circumpolar deepwater variability to northern hemisphere ice sheet melting?, Paleoceanography, 9, 661–675, https://doi.org/10.1029/93PA02199, 1994.

Osborne, E. B., Thunell, R. C., Marshall, B. J., Holm, J. A., Tappa, E. J., Benitez-Nelson, C., Cai, W.-J., and Chen, B.: Calcification of the planktonic foraminifera *Globigerina bulloides* and carbonate ion concentration: Results from the Santa Barbara Basin, Paleoceanography, 31, 1083–1102, https://doi.org/10.1002/2016PA002933, 2016.

Pagani, M.: Biomarker-based inferences of past climate: The alkenone pCO$_2$ Proxy, in: Treatise on Geochemistry, Elsevier, Oxford, 361–378, https://doi.org/10.1016/b978-0-08-095975-7.01027-5, 2014.

Pagani, M., Arthur, M. A., and Freeman, K. H.: Miocene evolution of atmospheric carbon dioxide, Paleoceanography, 14, 273–292, https://doi.org/10.1029/1999PA900006, 1999.

Pagani, M., Freeman, K. H., Ohkouchi, N., and Caldeira, K.: Comparison of water column [CO$_{2aq}$] with sedimentary alkenone-based estimates: A test of the alkenone-CO$_2$ proxy, Paleoceanography, 17, 21-21–21-12, https://doi.org/10.1029/2002pa000756, 2002.

Pagani, M., Zachos, J. C., Freeman, K. H., Tipple, B., and Bohaty, S.: Marked decline in atmospheric carbon dioxide concentrations during the Paleogene, Science, 309, 600–603, https://doi.org/10.1126/science.1110063, 2005.

Pagani, M., Liu, Z., LaRiviere, J., and Ravelo, A. C.: High Earth-system climate sensitivity determined from Pliocene carbon dioxide concentrations, Nat. Geosci., 3, 27–30, https://doi.org/10.1038/ngeo724, 2010.

Pagani, M., Huber, M., Liu, Z., Bohaty, S. M., Henderiks, J., Sijp, W., Krishnan, S., and DeConto, R. M.: The role of carbon dioxide during the onset of Antarctic Glaciation, Science, 334, 1261–1264, https://doi.org/10.1126/science.1203909, 2011.

Pahnke, K., Goldstein, S. L., and Hemming, S. R.: Abrupt changes in Antarctic Intermediate Water circulation over the past 25,000 years, Nat. Geosci., 1, 870–874, https://doi.org/10.1038/ngeo360, 2008.

Palmer, M. and Pearson, P. N.: A 23,000-year record of surface water pH and PCO$_2$ in the western equatorial Pacific Ocean, Science, 300, 480–482, https://doi.org/10.1126/science.1080796, 2003.

Palmer, M. R., Brummer, G. J., Cooper, M. J., Elderfield, H., Greaves, M. J., Reichart, G. J., Schouten, S., and Yu, J. M.: Multi-proxy reconstruction of surface water pCO$_2$ in the northern Arabian Sea since 29 ka, Earth Planet. Sc. Lett., 295, 49–57, https://doi.org/10.1016/j.epsl.2010.03.023, 2010.

Panieri, G., Lepland, A., Whitehouse, M. J., Wirth, R., Raanes, M. P., James, R. H., Graves, C. A., Crémière, A., and Schneider, A.: Diagenetic Mg-calcite overgrowths on foraminiferal tests in the vicinity of methane seeps, Earth Planet. Sc. Lett., 458, 203–212, https://doi.org/10.1016/j.epsl.2016.10.024, 2017.

Panmei, C., Divakar Naidu, P., and Mohtadi, M.: Bay of Bengal exhibits warming trend during the Younger Dryas: Implications of AMOC, Geochem. Geophy. Geosy., 18, 4317–4325, https://doi.org/10.1002/2017GC007075, 2017.

Parekh, P., Dutkiewicz, S., Follows, M. J., and Ito, T.: Atmospheric carbon dioxide in a less dusty world, Geophys. Res. Lett., 33, L03610, https://doi.org/10.1029/2005GL025098, 2006.

Partridge, T. C., Scott, L., and Hamilton, J. E.: Synthetic reconstructions of southern African environments during the Last Glacial Maximum (21–18 kyr) and the Holocene Altithermal (8–6 kyr), Quatern. Int., 57–58, 207–214, https://doi.org/10.1016/S1040-6182(98)00061-5, 1999.

Pedro, J. B., Bostock, H. C., Bitz, C. M., He, F., Vandergoes, M. J., Steig, E. J., Chase, B. M., Krause, C. E., Rasmussen, S. O., Markle, B. R., and Cortese, G.: The spatial extent and dynamics of the Antarctic Cold Reversal, Nat. Geosci., 9, 51–55, https://doi.org/10.1038/ngeo2580, 2016.

Peeters, F. J., Acheson, R., Brummer, G.-J. A., De Ruijter, W. P., Schneider, R. R., Ganssen, G. M., Ufkes, E., and Kroon, D.: Vigorous exchange between the Indian and Atlantic oceans at the end of the past five glacial periods, Nature, 430, 661–665, https://doi.org/10.1038/nature02785, 2004.

Peterson, R. G. and Stramma, L.: Upper-level circulation in the South Atlantic Ocean, Prog. Oceanogr., 26, 1–73, https://doi.org/10.1016/0079-6611(91)90006-8, 1991.

Pether, J.: Molluscan evidence for enhanced deglacial advection of Agulhas water in the Benguela current, off southwestern Africa, Palaeogeogr. Palaeocl., 111, 99–117, https://doi.org/10.1016/0031-0182(94)90350-6, 1994.

Petit, J. R., Jouzel, J., Raynaud, D., Barkov, N. I., Barnola, J. M., Basile, I., Bender, M., Chappellaz, J., Davis, M., Delaygue, G., Delmotte, M., Kotlyakov, V. M., Legrand, M., Lipenkov, V. Y., Lorius, C., Pépin, L., Ritz, C., Saltzman, E., and Stievenard, M.: Climate and atmospheric history of the past 420,000 years from the Vostok ice core, Antarctica, Nature, 399, 429–436, https://doi.org/10.1038/20859, 1999.

Popp, B. N., Laws, E. A., Bidigare, R. R., Dore, J. E., Hanson, K. L., and Wakeham, S. G.: Effect of phytoplankton cell geometry on carbon isotopic fractionation, Geochim. Cosmochim. Ac., 62, 69–77, https://doi.org/10.1016/S0016-7037(97)00333-5, 1998.

Pöppelmeier, F., Jeltsch-Thömmes, A., Lippold, J., Joos, F., and Stocker, T. F.: Multi-proxy constraints on Atlantic circulation dynamics since the last ice age, Nat. Geosci., 16, 349–356, https://doi.org/10.1038/s41561-023-01140-3, 2023.

Prahl, F. G. and Wakeham, S. G.: Calibration of unsaturation patterns in long-chain ketone compositions for palaeotemperature assessment, Nature, 330, 367–369, https://doi.org/10.1038/330367a0, 1987.

Rae, J. W. B., Zhang, Y. G., Liu, X., Foster, G. L., Stoll, H. M., and Whiteford, R. D. M.: Atmospheric CO$_2$ over the Past 66 Million Years from Marine Archives, Annu. Rev. Earth Pl. Sc., 49, 609–641, https://doi.org/10.1146/annurev-earth-082420-063026, 2021.

Rahmstorf, S.: Ocean circulation and climate during the past 120,000 years, Nature, 419, 207–214, https://doi.org/10.1038/nature01090, 2002.

Raitzsch, M., Bijma, J., Benthien, A., Richter, K.-U., Steinhoefel, G., and Kučera, M.: Boron isotope-based seasonal paleo-pH reconstruction for the Southeast Atlantic – A multispecies approach using habitat preference of planktonic foraminifera, Earth Planet. Sc. Lett., 487, 138–150, https://doi.org/10.1016/j.epsl.2018.02.002, 2018.

Rau, A. J., Rogers, J., Lutjeharms, J. R. E., Giraudeau, J., Lee-Thorp, J. A., Chen, M. T., and Waelbroeck, C.: A 450-kyr record of hydrological conditions on the western Agulhas Bank Slope, south of Africa, Mar. Geol., 180, 183–201, https://doi.org/10.1016/S0025-3227(01)00213-4, 2002.

Rau, G. H., Riebesell, U., and Wolf-Gladrow, D.: A model of photosynthetic ^{13}C fractionation by marine phytoplankton based on diffusive molecular CO$_2$ uptake, Mar. Ecol. Prog. Ser., 133, 275–285, https://doi.org/10.3354/meps133275, 1996.

Rebotim, A., Voelker, A. H. L., Jonkers, L., Waniek, J. J., Meggers, H., Schiebel, R., Fraile, I., Schulz, M., and Kucera, M.: Factors controlling the depth habitat of planktonic foraminifera in the subtropical eastern North Atlantic, Biogeosciences, 14, 827–859, https://doi.org/10.5194/bg-14-827-2017, 2017.

Redfield, A. C.: The biological control of chemical factors in the environment, Am. Sci., 46, 205–221, https://www.jstor.org/stable/27827150 (last access: 19 March 2025), 1958.

Regenberg, M., Nürnberg, D., Steph, S., Groeneveld, J., Garbe-Schönberg, D., Tiedemann, R., and Dullo, W. C.: Assessing the effect of dissolution on planktonic foraminiferal Mg / Ca ratios: Evidence from Caribbean core tops, Geochem. Geophy. Geosy., 7, Q07P15, https://doi.org/10.1029/2005GC001019, 2006.

Reinfelder, J. R.: Carbon concentrating mechanisms in eukaryotic marine phytoplankton, Ann. Rev. Mar. Sci., 3, 291–315, https://doi.org/10.1146/annurev-marine-120709-142720, 2011.

Riebesell, U., Revill, A. T., Holdsworth, D. G., and Volkman, J. K.: The effects of varying CO_2 concentration on lipid composition and carbon isotope fractionation in *Emiliania huxleyi*, Geochim. Cosmochim. Ac., 64, 4179–4192, https://doi.org/10.1016/S0016-7037(00)00474-9, 2000.

Romanek, C. S., Grossman, E. L., and Morse, J. W.: Carbon isotopic fractionation in synthetic aragonite and calcite: Effects of temperature and precipitation rate, Geochim. Cosmochim. Ac., 56, 419–430, https://doi.org/10.1016/0016-7037(92)90142-6, 1992.

Romero, O., Mollenhauer, G., Schneider, R., and Wefer, G.: Oscillations of the siliceous imprint in the central Benguela Upwelling System from MIS 3 through to the early Holocene: The influence of the Southern Ocean, J. Quaternary Sci., 18, 733–743, https://doi.org/10.1002/jqs.789, 2003.

Ronge, T. A., Steph, S., Tiedemann, R., Prange, M., Merkel, U., Nürnberg, D., and Kuhn, G.: Pushing the boundaries: Glacial/interglacial variability of intermediate and deep waters in the southwest Pacific over the last 350,000 years, Paleoceanography, 30, 23–38, https://doi.org/10.1002/2014PA002727, 2015.

Roobaert, A., Laruelle, G. G., Landschützer, P., Gruber, N., Chou, L., and Regnier, P.: The spatiotemporal dynamics of the sources and sinks of CO_2 in the global coastal ocean, Global Biogeochem. Cy., 33, 1693–1714, https://doi.org/10.1029/2019GB006239, 2019.

Rühlemann, C., Mulitza, S., Müller, P. J., Wefer, G., and Zahn, R.: Warming of the tropical Atlantic Ocean and slowdown of thermohaline circulation during the last deglaciation, Nature, 402, 511–514, https://doi.org/10.1038/990069, 1999.

Salt, L. A., van Heuven, S. M. A. C., Claus, M. E., Jones, E. M., and de Baar, H. J. W.: Rapid acidification of mode and intermediate waters in the southwestern Atlantic Ocean, Biogeosciences, 12, 1387–1401, https://doi.org/10.5194/bg-12-1387-2015, 2015.

Santana-Casiano, J. M., González-Dávila, M., and Ucha, I. R.: Carbon dioxide fluxes in the Benguela upwelling system during winter and spring: A comparison between 2005 and 2006, Deep-Sea Res. Pt. II, 56, 533–541, https://doi.org/10.1016/j.dsr2.2008.12.010, 2009.

Sarnthein, M., Winn, K., Jung, S. J. A., Duplessy, J.-C., Labeyrie, L., Erlenkeuser, H., and Ganssen, G.: Changes in East Atlantic Deepwater Circulation over the last 30,000 years: Eight time slice reconstructions, Paleoceanography, 9, 209–267, https://doi.org/10.1029/93PA03301, 1994.

Schlitzer, R.: eWOCE-Electronic Atlas of WOCE Data, WOCE Global Data, Version 2.0 CD-ROM, WOCE Intern. Project Office, WOCE Report No. 171/00, Southampton, UK, https://doi.org/10013/epic.14768, 2000.

Schmittner, A., Gruber, N., Mix, A. C., Key, R. M., Tagliabue, A., and Westberry, T. K.: Biology and air–sea gas exchange controls on the distribution of carbon isotope ratios (δ^{13}C) in the ocean, Biogeosciences, 10, 5793–5816, https://doi.org/10.5194/bg-10-5793-2013, 2013.

Schouten, S., Klein Breteler, W. C. M., Blokker, P., Schogt, N., Rijpstra, W. I. C., Grice, K., Baas, M., and Sinninghe Damsté, J. S.: Biosynthetic effects on the stable carbon isotopic compositions of algal lipids: implications for deciphering the carbon isotopic biomarker record, Geochim. Cosmochim. Ac., 62, 1397–1406, https://doi.org/10.1016/S0016-7037(98)00076-3, 1998.

Scussolini, P. and Peeters, F. J.: A record of the last 460 thousand years of upper ocean stratification from the central Walvis Ridge, South Atlantic, Paleoceanography, 28, 426–439, https://doi.org/10.1002/palo.20041, 2013.

Seki, O., Foster, G. L., Schmidt, D. N., Mackensen, A., Kawamura, K., and Pancost, R. D.: Alkenone and boron-based Pliocene pCO$_2$ records, Earth Planet. Sc. Lett., 292, 201–211, https://doi.org/10.1016/j.epsl.2010.01.037, 2010.

Sexton, P. F., Wilson, P. A., and Pearson, P. N.: Microstructural and geochemical perspectives on planktic foraminiferal preservation: "Glassy" versus "Frosty", Geochem. Geophy. Geosy., 7, Q12P19, https://doi.org/10.1029/2006gc001291, 2006.

Shannon, L. and Nelson, G.: The Benguela: large scale features and processes and system variability, in: The south atlantic, Springer, Berlin, Heidelberg, 163–210, https://doi.org/10.1007/978-3-642-80353-6_9, 1996.

Shannon, L. V. and O'Toole, M.: Sustainability of the Benguela: ex Africa semper aliquid novi, in: Large Marine Ecosystems of the World: Trends in Exploitation, Protection and Research, edited by: Hempel, G. and Sherman, K., Elsevier B.V., Amsterdam, 227–253, 978-0444510273, 2003.

Shi, N., Dupont, L. M., Beug, H.-J., and Schneider, R.: Vegetation and climate changes during the last 21 000 years in S.W. Africa based on a marine pollen record, Veg. Hist. Archaeobot., 7, 127–140, https://doi.org/10.1007/BF01374001, 1998.

Shillington, F.: The Benguela upwelling system off southwestern Africa, Sea, 11, 583–604, 1998.

Spero, H. J.: Do planktic foraminifera accurately record shifts in the carbon isotopic composition of seawater ΣCO$_2$?, Mar. Micropaleontol., 19, 275–285, https://doi.org/10.1016/0377-8398(92)90033-G, 1992.

Spero, H. J. and Lea, D. W.: Intraspecific stable isotope variability in the planktic foraminifera *Globigerinoides sacculifer*: Results from laboratory experiments, Mar. Micropaleontol., 22, 221–234, https://doi.org/10.1016/0377-8398(93)90045-Y, 1993.

Spero, H. J. and Lea, D. W.: Experimental determination of stable isotope variability in *Globigerina bulloides*: implications for paleoceanographic reconstructions, Mar. Micropaleontol., 28, 231–246, https://doi.org/10.1016/0377-8398(96)00003-5, 1996.

Spero, H. J., Bijma, J., Lea, D. W., and Bemis, B. E.: Effect of seawater carbonate concentration on foraminiferal carbon and oxygen isotopes, Nature, 390, 497–500, https://doi.org/10.1038/37333, 1997.

Stainbank, S., Spezzaferri, S., De Boever, E., Bouvier, A.-S., Chilcott, C., De Leau, E. S., Foubert, A., Kunkelova, T., Pichevin, L., Raddatz, J., Rüggeberg, A., Wright, J. D., Yu, S. M., Zhang, M., and Kroon, D.: Assessing the impact of diagenesis on foraminiferal geochemistry from a low latitude, shallow-water drift deposit, Earth Planet. Sc. Lett., 545, 116390, https://doi.org/10.1016/j.epsl.2020.116390, 2020.

Stephens, B. B. and Keeling, R. F.: The influence of Antarctic sea ice on glacial–interglacial CO_2 variations, Nature, 404, 171–174, https://doi.org/10.1038/35004556, 2000.

Stocker, T. F.: The Seesaw Effect, Science, 282, 61–62, https://doi.org/10.1126/science.282.5386.61, 1998.

Stoll, H. M., Guitian, J., Hernandez-Almeida, I., Mejia, L. M., Phelps, S., Polissar, P., Rosenthal, Y., Zhang, H., and Ziveri, P.: Upregulation of phytoplankton carbon concentrating mechanisms during low CO_2 glacial periods and implications for the phytoplankton pCO$_2$ proxy, Quaternary Sci. Rev., 208, 1–20, https://doi.org/10.1016/j.quascirev.2019.01.012, 2019.

Stramma, L. and England, M.: On the water masses and mean circulation of the South Atlantic Ocean, J. Geophys. Res.-Oceans, 104, 20863–20883, https://doi.org/10.1029/1999JC900139, 1999.

Stuut, J.-B. W., Prins, M. A., Schneider, R. R., Weltje, G. J., Jansen, J. H. F., and Postma, G.: A 300-kyr record of aridity and wind strength in southwestern Africa: inferences from grain-size distributions of sediments on Walvis Ridge, SE Atlantic, Mar. Geol., 180, 221–233, https://doi.org/10.1016/S0025-3227(01)00215-8, 2002.

Suggate, R. P. and Almond, P. C.: The Last Glacial Maximum (LGM) in western South Island, New Zealand: implications for the global LGM and MIS 2, Quaternary Sci. Rev., 24, 1923–1940, https://doi.org/10.1016/j.quascirev.2004.11.007, 2005.

Synal, H.-A., Stocker, M., and Suter, M.: MICADAS: A new compact radiocarbon AMS system, Nucl. Instrum. Meth. B, 259, 7–13, https://doi.org/10.1016/j.nimb.2007.01.138, 2007.

Tapia, R., Ho, S. L., Wang, H.-Y., Groeneveld, J., and Mohtadi, M.: Contrasting vertical distributions of recent planktic foraminifera off Indonesia during the southeast monsoon: implications for paleoceanographic reconstructions, Biogeosciences, 19, 3185–3208, https://doi.org/10.5194/bg-19-3185-2022, 2022.

Thomas, E. and Shackleton, N. J.: The Paleocene-Eocene benthic foraminiferal extinction and stable isotope anomalies, Geological Society, London, Special Publications, 101, 401–441, https://doi.org/10.1144/GSL.SP.1996.101.01.20, 1996.

Tian, H.-A., van Manen, M., Bunnell, Z. B., Jung, J., Lee, S. H., Kim, T.-W., Reichart, G.-J., Conway, T. M., and Middag, R.: Biogeochemistry of iron in coastal Antarctica: isotopic insights for external sources and biological uptake in the Amundsen Sea polynyas, Geochim. Cosmochim. Ac., 363, 51–67, https://doi.org/10.1016/j.gca.2023.10.029, 2023.

Turi, G., Lachkar, Z., and Gruber, N.: Spatiotemporal variability and drivers of pCO$_2$ and air–sea CO_2 fluxes in the California Current System: an eddy-resolving modeling study, Biogeosciences, 11, 671–690, https://doi.org/10.5194/bg-11-671-2014, 2014.

Turner, J. T.: Zooplankton fecal pellets, marine snow, phytodetritus and the ocean's biological pump, Prog. Oceanogr., 130, 205–248, https://doi.org/10.1016/j.pocean.2014.08.005, 2015.

Umling, N. E., Oppo, D. W., Chen, P., Yu, J., Liu, Z., Yan, M., Gebbie, G., Lund, D. C., Pietro, K. R., Jin, Z. D., Huang, K. F., Costa, K. B., and Toledo, F. A. L.: Atlantic circulation and ice sheet influences on upper South Atlantic temperatures during the Last Deglaciation, Paleoceanogr. Paleocl., 34, 990–1005, https://doi.org/10.1029/2019PA003558, 2019.

Vandergoes, M. J., Dieffenbacher-Krall, A. C., Newnham, R. M., Denton, G. H., and Blaauw, M.: Cooling and changing seasonality in the Southern Alps, New Zealand during the Antarctic Cold Reversal, Quaternary Sci. Rev., 27, 589–601, https://doi.org/10.1016/j.quascirev.2007.11.015, 2008.

Van Dijk, I., de Nooijer, L. J., Wolthers, M., and Reichart, G.-J.: Impacts of pH and $[CO_3^{2-}]$ on the incorporation of Zn in foraminiferal calcite, Geochim. Cosmochim. Ac., 197, 263–277, https://doi.org/10.1016/j.gca.2016.10.031, 2017.

van Dongen, B. E., Schouten, S., and Damsté, J. S. S.: Carbon isotope variability in monosaccharides and lipids of aquatic algae and terrestrial plants, Mar. Ecol. Prog. Ser., 232, 83–92, https://doi.org/10.3354/meps232083, 2002.

Volk, T. and Hoffert, M. I.: Ocean carbon pumps: Analysis of relative strengths and efficiencies in ocean-driven atmospheric CO_2 changes, in: The carbon cycle and atmospheric CO_2: Natural variations archean to present, Geoph. Monog. Series, 32, 99–110, https://doi.org/10.1029/GM032p0099, 1985.

Wacker, L., Fahrni, S. M., Hajdas, I., Molnar, M., Synal, H. A., Szidat, S., and Zhang, Y. L.: A versatile gas interface for routine radiocarbon analysis with a gas ion source, Nucl. Instrum. Meth. B, 294, 315–319, https://doi.org/10.1016/j.nimb.2012.02.009, 2013.

Wacker, L., Güttler, D., Goll, J., Hurni, J. P., Synal, H. A., and Walti, N.: Radiocarbon dating to a single year by means of rapid atmospheric ^{14}C changes, Radiocarbon, 56, 573–579, https://doi.org/10.2458/56.17634, 2014.

Waelbroeck, C., Labeyrie, L., Michel, E., Duplessy, J. C., McManus, J. F., Lambeck, K., Balbon, E., and Labracherie, M.: Sea-level and deep water temperature changes derived from benthic foraminifera isotopic records, Quaternary Sci. Rev., 21, 295–305, https://doi.org/10.1016/S0277-3791(01)00101-9, 2002.

Wang, B.-S., You, C.-F., Huang, K.-F., Wu, S.-F., Aggarwal, S. K., Chung, C.-H., and Lin, P.-Y.: Direct separation of boron from Na- and Ca-rich matrices by sublimation for stable isotope measurement by MC-ICP-MS, Talanta, 82, 1378–1384, https://doi.org/10.1016/j.talanta.2010.07.010, 2010.

Wang, Y. V., Leduc, G., Regenberg, M., Andersen, N., Larsen, T., Blanz, T., and Schneider, R. R.: Northern and southern hemisphere controls on seasonal sea surface temperatures in the Indian Ocean during the last deglaciation, Paleoceanography, 28, 619–632, https://doi.org/10.1002/palo.20053, 2013.

Wefer, G. A., Berger, W. H., Bickert, T., Donner, B., Fischer, G., von Mücke, S. K., Meinecke, G., Müller, P., Mulitza, S., and Niebler, H.-S.: Late Quaternary surface circulation of the South Atlantic: The stable isotope record and implications for heat transport and productivity, in: The South Atlantic, Springer, Berlin, Heidelberg, 461–502, https://doi.org/10.1007/978-3-642-80353-6_25, 1996.

Weltje, G. J. and Tjallingii, R.: Calibration of XRF core scanners for quantitative geochemical logging of sediment cores: Theory and application, Earth Planet. Sc. Lett., 274, 423–438, https://doi.org/10.1016/j.epsl.2008.07.054, 2008.

Wilkes, E. B. and Pearson, A.: A general model for carbon isotopes in red-lineage phytoplankton: Interplay between unidirectional processes and fractionation by RubisCO, Geochim. Cosmochim. Ac., 265, 163–181, https://doi.org/10.1016/j.gca.2019.08.043, 2019.

Witkowski, C. R., Weijers, J. W., Blais, B., Schouten, S., and Damsté, J. S. S.: Molecular fossils from phytoplankton reveal secular PCO$_2$ trend over the Phanerozoic, Sci. Adv., 4, eaat4556, https://doi.org/10.1126/sciadv.aat4556, 2018.

Witkowski, C. R., van der Meer, M. T., Blais, B., Damsté, J. S. S., and Schouten, S.: Algal biomarkers as a proxy for pCO$_2$: Constraints from late quaternary sapropels in the eastern Mediterranean, Org. Geochem., 150, 104123, https://doi.org/10.1016/j.orggeochem.2020.104123, 2020.

Zeebe, R. E. and Wolf-Gladrow, D.: CO$_2$ in seawater: Equilibrium, kinetics, isotopes, Elsevier Oceanography Series, 65, Elsevier, Amsterdam, 978-0444509468, 2001.

Zeebe, R. E., Bijma, J., and Wolf-Gladrow, D. A.: A diffusion-reaction model of carbon isotope fractionation in foraminifera, Mar. Chem., 64, 199–227, https://doi.org/10.1016/S0304-4203(98)00075-9, 1999.

Zhang, Y. G., Pagani, M., Liu, Z., Bohaty, S. M., and DeConto, R.: A 40-million-year history of atmospheric CO$_2$, Philos. T. Roy. Soc. A, 371, 20130096, https://doi.org/10.1098/rsta.2013.0096, 2013.

Zhang, Y. G., Pearson, A., Benthien, A., Dong, L., Huybers, P., Liu, X., and Pagani, M.: Refining the alkenone-pCO$_2$ method I: Lessons from the Quaternary glacial cycles, Geochim. Cosmochim. Ac., 260, 177–191, https://doi.org/10.1016/j.gca.2019.06.032, 2019.

Zhang, Y. G., Henderiks, J., and Liu, X.: Refining the alkenone-pCO$_2$ method II: Towards resolving the physiological parameter "b", Geochim. Cosmochim. Ac., 281, 118–134, https://doi.org/10.1016/j.gca.2020.05.002, 2020.